ISSN 0973-3302

THE JOURNAL OF ACOUSTICAL SOCIETY OF INDIA

Volume 52 Number 4 October 2025

A Quarterly Publication of the ASI
https://acoustics.org.in

The Journal of Acoustical Society of India

Volume 52 Number 4 October 2025 pp 165-203

ASI

The Journal of Acoustical Society of India

The Refereed Journal of the Acoustical Society of India (JASI)

The Journal of Acoustical Society of India is a refereed journal of the Acoustical Society of India **(ASI)**. The **ASI** is a non-profit national society founded in 31st July, 1971. The primary objective of the society is to advance the science of acoustics by creating an organization that is responsive to the needs of scientists and engineers concerned with acoustics problems all around the world.

Manuscripts of articles, technical notes and letter to the editor should be submitted to the Chief Editor. Copies of articles on specific topics listed above should also be submitted to the respective Associate Scientific Editor. Manuscripts are refereed by at least two referees and are reviewed by Publication Committee (all editors) before acceptance. On acceptance, revised articles with the text and figures scanned as separate files on a diskette should be submitted to the Editor by express mail. Manuscripts of articles must be prepared in strict accordance with the author instructions.

All information concerning subscription, new books, journals, conferences, etc. should be submitted to Chief Editor:

B. Chakraborty, CSIR - National Institute of Oceanography, Dona Paula, Goa-403 004,
Tel: +91.832.2450.318, Fax: +91.832.2450.602, e-mail: bishwajit@nio.org

Annual subscription price including mail postage is Rs. 2500/= for institutions, companies and libraries and Rs. 2500/= for individuals who are not **ASI** members. The Journal of Acoustical Society of India will be sent to **ASI** members free of any extra charge. Requests for specimen copies and claims for missing issues as well as address changes should be sent to the Editorial Office:

ASI Secretariat, C/o Acoustics and Vibration Metrology, CSIR-National Physical Laboratory, Dr. KS Krishnan Road, New Delhi 110 012, Tel: +91.11.4560.8317, Fax: +91.11.4560.9310, e-mail: asisecretariat.india@gmail.com

ISSN 0973-3302

Printed at Alpha Printers, WZ-35/C, Naraina, Near Ring Road, New Delhi-110028 Tel.: 9810804196. JASI is sent to ASI members free of charge.

ASI

The Journal of Acoustical Society of India

A quarterly publication of the Acoustical Society of India

Volume 52, Number 4, October 2025

ARTICLES

INFORMATION

FOREWORD

This special issue of JASI is a collection of selected papers presented in the 51st National Symposium of Acoustics (NSA-2024) organized by NSTL, Visakhapatnam during 27-28 Aug 2024 with a theme of “Sustainable Acoustics”. The papers presented at NSA-2024 provide a comprehensive representation of current research efforts and progress made in the past few years. The papers indicate a high level of research interest which has led to significant advancements in acoustic sensing, modeling and measurement technologies and highlight the most promising trends for future research.

The five papers selected for publication in this issue encompassa variety of interesting research topics in the field of underwater acoustics such as acoustic wave properties of sandy sediments, seasonal variability of transmission loss with variable range-dependent bathymetry, emerging transducer technologies, and autonomous underwater vehicle (AUV) based detection, localization and classification of mine-like objects (MLOs).

The first paper estimates the geoacoustic wave properties of coarse sandy sediments obtained from Idukki reservoir in Kerala based on the laboratory analysis of the sediment samples for the geophysical properties such as mean grain size, porosity, and wet bulk density (A. T. Sivadas and S. Radhakrishnan). The second paper models and discusses the effect of seasonal variability of sound speed profile on upslope and downslope transmission loss utilizing a parabolic equation model (Elizabeth Shani *et al.*). Balamurugan *et al.* discuss the survey, design and performance evaluation of an Indigenous very low frequency electromagnetic projector to obtain higher source level at lower frequencies. The next paper investigates the acceleration sensitivity of hydrophone for different mounting configurations presents research findings on optimizing hydrophone performance based on a finite element approach (Sulthan *et al.*). The paper by Amit Kumar Verma discusses the approach for AUV based mine countermeasures using content-based image retrieval.

On behalf of all the authors, we express our gratitude to the chief editor of JASI and ASI for providing us an opportunity to publish our findings. We sincerely appreciate the meticulous and selfless efforts of the reviewers, who rigorously examined all the manuscripts. Their invaluable feedback has significantly helped in improving the quality of the papers.

Dr. Sreeram Radhakrishnan
Naval Physical and Oceanographic Laboratory, Kochi, India
Guest Editor

The Journal of Acoustical Society of India : Vol. 52, No. 4, 2025 (pp. 167-174)

Analysis of geoacoustic wave properties of coarse sandy sediments obtained from Idukki reservoir

Akshara T. Sivadas[1,2] and Sreeram Radhakrishnan[1]
[1]Naval Physical & Oceanographic Laboratory, Kochi-682 021, India
[2]*Cochin University of Science and Technology, Kochi-682 016*, India
e-mail: tsakshara@gmail.com

[Received: 01.09.2025; Revised: 21.09.2025; Accepted: 24.09.2025]

ABSTRACT

For modelling acoustic wave propagation in hard consolidated sediments, it is essential to estimate the geophysical properties of the sediment. In this research work, sediment samples collected from three locations in the riverbed of Idukki reservoir in Kerala, are analysed in the laboratory to measure the geophysical properties such as mean grain size, porosity, and wet bulk density. These properties are used to estimate the geoacoustical parameters like compressional (longitudinal) velocity and compressional attenuation which acts as input for geoacoustical models. The geoacoustical parameters are predicted utilizing the theoretical acoustic wave propagation models like effective density fluid model (EDFM), grain shearing (GS) and viscous grain shearing model (VGS) model which helps in predicting the acoustic wave propagation. The geophysical property of the sediment samples in site 1 is found to be very denser compared to sediments from site 2 and 3 which are fine medium sand type. The estimated compressional velocity from EDFM, GS, and VGS models at site 1 has higher compressional velocity at which is possibly due to low porosity of the sediments. The attenuation is observed to be high for more porous sediment samples. It is observed that denser sediments contribute to lower sound attenuation.

1. INTRODUCTION

In the present analysis, sediment samples are collected from 3 different shallow water test sites region in Idukki reservoir where mine-like objects (MLO) were buried under the soil for the conduct of acoustic wave experiments. Extraction of soil samples near the surface is carried out at desired depths to mainly investigate the geophysical properties of sediment like soil type, mean grain size, sediment size distribution, porosity, and wet bulk density. These properties can be estimated in the laboratory via standard measuring techniques. The published literature indicates that the dispersion relationships for the phase speed and the sediment attenuation through the sediment layer depends mainly on porosity, mean grain size and depth of the sediment layer[1]. The other properties which are constants like tortuosity, permeability attributes to the microscopic level changes happening at the grain-to-grain contact. The geophysical properties can yield the geoacoustic properties utilizing established empirical equations that help in predicting the nature of dissipation of sound signals when it travels through soil[2]. The objective of the present analysis is to determine the compressional wave properties of the sediment samples based on different existing theoretical models. In this research work, the methods of effective density fluid model[3], grain-shearing model[4] and viscous grain-shearing model[5] are implemented and the results are discussed.

2. MATERIALS AND METHODS

2.1 Mean Grain Size Analysis

The geophysical properties of sediment samples obtained from the three sites are estimated in the laboratory. The properties include porosity, wet bulk density and mean grain size. The sediment texture is determined by the gradistat software which is widely used to generate the weight distribution of the sediment data using the laser granulometer or sieve. The sample analysed is obtained to be poorly sorted and polymodal in texture. The mean grain size is computed using Folk and Ward method (1957)[6]. Mean grain size is measured in logarithmic phi units and it is the most widely compared parameter.

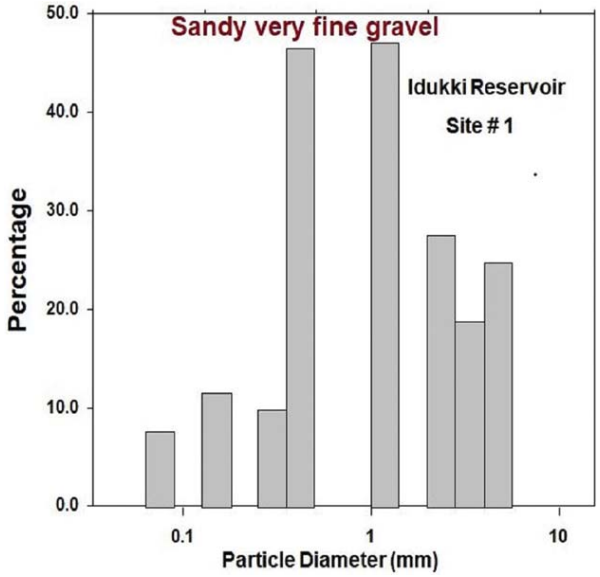

Fig. 1 : Sediment weight distribution in the sample obtained from site #1 in Idukki Reservoir. The sediment is classified as **Sandy very fine gravel** based on the mean grain size

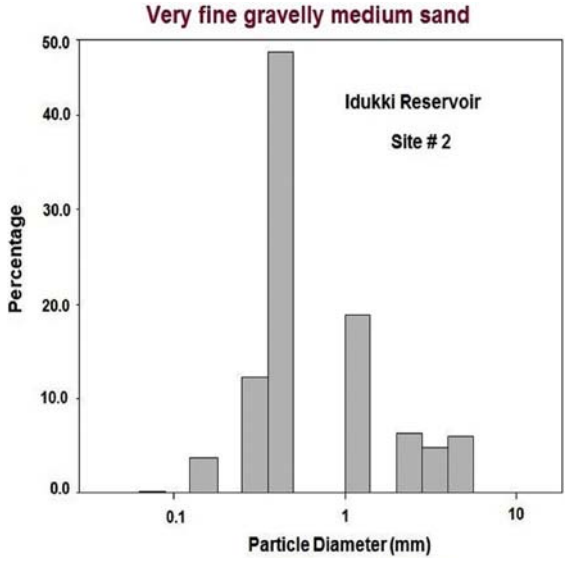

Fig. 2 : Sediment weight distribution in the sample obtained from site #2 in Idukki Reservoir. The sediment is classified as **Very fine gravelly medium sand** based on the mean grain size.

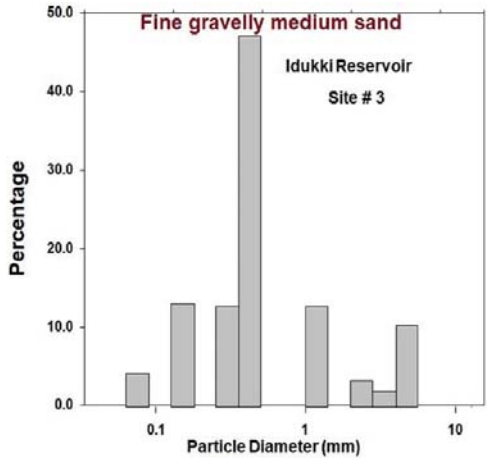

Fig. 3 : Sediment weight distribution in the sample obtained from site #3 in Idukki Reservoir. The sediment is classified as **Fine gravelly medium sand** based on the mean grain size.

The porosity-density computation is achieved using the classic methodology of pyncnometer. It is estimated using the weight volume method.

The diameter of the particle is given by $d\ (mm) = 2^{-\Phi}$

$$\Phi = -\log_2 d\ (mm) \tag{1}$$

Table 1. Measured geophysical parameters in site 1-3

Site No.	Porosity	Wet Bulk Density (kg/m^3)	Mean Size Grain
1	0.13	2.35	-1.833
2	0.44	1.71	0.5267
3	0.35	2.06	1.1233

3. WAVE PROPERTIES OF SEDIMENTS

There are two major physical mechanisms which explain the attenuation of the sound as it passes through the sandy sediment. The first mechanism was proposed by Biot which was later applied mathematically by Stoll[7] using the poroelastic theory. In this theory viscosity plays a significant role in the dissipation of acoustic signal. The attenuation in the sediments varies as the square of the frequency for low frequency bands and for the high frequency ranges attenuation varies as the square root of the frequencies which contradicts some of the measurements.

The second mechanism which governs the sound attenuation within the sediment is due to the interaction between the sand grains at the grain contacts. Buckingham theory predicts the sound attenuation is linear with respect to the frequency while the sound speed exhibits very little dispersion. This model only fits well with higher frequency than the lower frequency measurements. In the Biot model, relative motion of the pore fluid and the sand grains is the key physical effect, whereas in the Buckingham theory, the shearing of the grain contacts is the reason for the dissipation of the compressional wave.

3.1 Effective Density Fluid Model (Simplified Biot theory)

The Biot-Stoll model can be cumbersome to implement as it requires 13 material parameters as inputs. Many of these material parameters are difficult to measure. To mitigate these difficulties, Williams[8] proposed effective density fluid model (EDFM) which provides a simpler alternative to the Biot theory.

The EDFM requires a total of 8 input parameters. This model predicts one dimensional compressional wave in the sediment and is compatible with the Rayleigh reflection loss at the water-sediment interface because the effective density compensates for the Biot slow wave theory. The dispersion, transmission, reflection and scattering of the effective density fluid model are almost similar to the Biot-Stoll theory. Biot-Stoll model for poroelastic media, penetration at shallow grazing angles could be explained by the existence of the Biot slow wave. The compressional velocity, c_p is derived by the expressions below:

Biot assumed the shape of the pores as cylindrical in nature,

$$F(\varepsilon)=\frac{\frac{\varepsilon}{4}T(\varepsilon)}{1-\frac{2i}{\varepsilon}T(\varepsilon)}$$, j_o and j_1 are Bessel cylindrical functions

$$T(\varepsilon)=\frac{\left(-\sqrt{i}\right)J_1\left(\varepsilon\sqrt{i}\right)}{J_o\left(\varepsilon\sqrt{i}\right)} \tag{2}$$

$\varepsilon = a\sqrt{\frac{\omega\rho f}{\eta}}$, where a is pore size parameter

The pore size a is considered unchanged

$\varepsilon = a\sqrt{\frac{8\alpha\kappa}{\beta}}$, a is the pore radius

The complex effective density is given by the formula:

$$\rho_{eff} = \rho_f\left(\frac{\alpha(1-\beta)\rho s + \beta(\alpha-1)\rho_f + \frac{i\beta\rho F\eta}{\rho f\omega\kappa}}{\beta(1-\beta)\rho s+(\alpha-2\beta+\beta^2)\rho_f+\frac{i\beta F\eta}{\omega\kappa}}\right) \tag{3}$$

Bulk modulus of frame and shear modulus of frame are taken to be zero

Taking $$K_b = \mu = 0,\ H = C = M = \left(\frac{(1-\beta)}{K_r} + \frac{\beta}{K_f}\right)^{-1} \tag{4}$$

Eqn. 4 states that the compressibility (inverse of modulus) is a linear function of the concentration of the particles in a suspension.

$$c_p = \sqrt{H/\rho_{eff}} \tag{5}$$

The final expression for attenuation $\alpha_p(\mathrm{dB/m})$ is obtained as

$$\alpha_p = 8.686\omega\cdot \mathrm{Im}\sqrt{\rho_{eff}/K_{eff}} \tag{6}$$

3.2 Grain Shearing Model

The sedimentary rocks saturated with pore fluid form an elastic matrix or skeletal frame. This consolidated pack of water bounded granular material acts as a medium for the passage of the slow and

fast moving waves. The presence of the compressible viscous fluid within the pores makes the mobility of the grains easier. Such dynamical behaviour of the sediment gives rise to grain-to-grain interactions. Inter-granular shearing in the sediment results in a process known as the "stick-slip". Though the Buckingham theory suggests a grain-to-grain shearing model, it has been recently modified to incorporate a linear loss mechanism at the grain contacts. The other parameters considered for the model prediction are bulk modulus of the pore fluid According to Buckingham, G-S Dispersion relation for the compressional speed c_p is given by the expressions:

$$c_p = \frac{c_0}{\mathrm{Re}\left[1+\frac{\rho_p+\left(4/3\right)\gamma_s}{c_o^2\,\rho_o}\left(j\omega T\right)^n\right]^{-1/2}} \tag{7}$$

$c_0 = \sqrt{\frac{K_0}{\rho_0}}$, Wood's equation, sound speed without inter grain interaction and K_o is the bulk moduli of the pore water.

$$X = \frac{\gamma_p + (4/3)\gamma_s}{c_0^2\rho_0} \tag{8}$$

Where, *X* represents dimensionless G-S coefficient. γ_s and γ_p are the shear and the compressional coefficient. The attenuation α_p (dB/m) is given by:

$$\alpha_p = -\frac{\omega}{c_o}\mathrm{Im}\left[1+\frac{\rho_p+\left(4/3\right)\gamma_s}{c_o^2\,\rho_o}\left(j\omega T\right)^n\right]^{-1/2} \tag{9}$$

Where, *n* is the strain hardening index.

3.3 Viscous Grain Shearing (VGS) Model

The grain-shearing model (G-S) of compressional wave propagation in a saturated granular material is further extended to include the effects of the viscosity of the thin layer of the pore fluid separating known as the viscous grain shearing model (VGS). It is predicted that the VGS theory at lower frequencies, below 10 kHz, the effects due to viscosity of the pore fluid may be non-negligible. At higher frequencies, the VGS dispersion curves matches with the G-S theory asymptotically. The expression for the compressional velocity is the ratio of wood's equation to the real part of the effect of the dissipation of the viscous force which is combined with the rigidity coefficient ($\gamma_T = \gamma_p + (4/3)\gamma_s$) and material exponent, *n*. It is derived by the following expression given below:

$$c_p = \frac{c_0}{\mathrm{Re}\left[1+g(\omega)\frac{\gamma_p+\left(4/3\right)\gamma_s}{c_o^2\,\rho_o}\left(j\omega T\right)^n\right]^{-1/2}} \tag{10}$$

$$g(\omega) = \left(1+\frac{1}{j\omega T}\right)^{-1+n} \tag{11}$$

Where, $g(\omega)$ is the effect of viscous dissipation, T is the arbitrary time taken as unity.

The compressional attenuation α_p (dB/m) is obtained by the expression:

$$\alpha_p = -\frac{\omega}{c_o}\mathrm{Im}\left[1+\frac{\gamma_p+\left(4/3\right)\gamma_s}{c_o^2\,\rho_o}\left(j\omega T\right)^n\right]^{-1/2} \tag{12}$$

4. ANALYSIS : RESULTS AND DISCUSSIONS

In this section, compressional sound speed and attenuations of sediments obtained from 3 sites in the Idukki reservoir are estimated and the results are discussed. The published results from SAX99[1] are used as a benchmark for the verification of results. The theoretical wave dispersion of wave speed for SAX99 for plotted for EDFM, GS and VGS models. SAX99 is a high frequency sediment acoustic experiment conducted in an effort to determine the geoacoustical properties of the sandy sediments. It was conducted for a frequency band between 125 Hz to 400 kHz and sediment attenuation was measured over a frequency range of 2.6 to 400 kHz[2]. The theoretical wave speed for SAX99 sediment experiment ranges between 1700 to 1820 m/s. For modelling the dispersion relation, empirical evaluation of the other constant parameters like pore fluid density (ρ_w = 1000 to 1026 kg/m^3), shear coefficient (γ_s = 4.588 × 10^7 Pa), compressional coefficient (γ_p = 3.888 × 10^8 Pa), strain-hardening index (n ranging from 0.0851 to 0.0901), permeability (k = 1 × 10^{-10} m^2), bulk modulus of pore fluid (k_f = 2.25 × 10^9 to 2.4 × 10^9 Pa), bulk modulus of the sand grain (k_s = 3.2 to 3.6 × 10^{10} Pa) and grain roughness (δ = 1μm) are also considered to predict the values of the compressional velocity and compressional attenuation. These are the parameter values utilized to compute the EDFM, G-S and VGS model results.

4.1 Compressional Velocity

There is an initial increase of velocity for low frequency ranges but the velocity tends to be constant when frequency increases. The geoacoustic parameters are estimated from the geophysical properties of

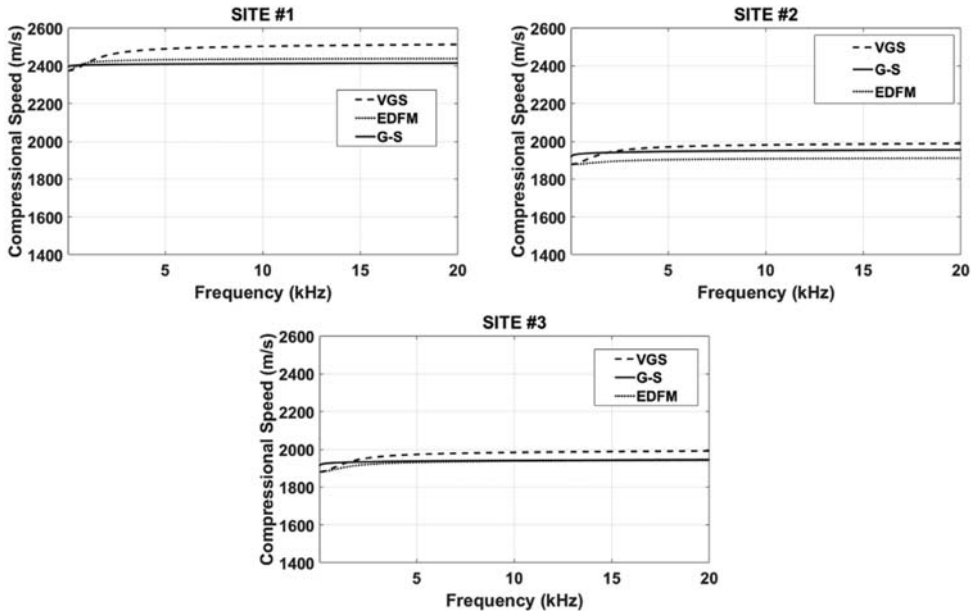

Fig. 4: The compressional velocity predicted for Grain shearing model, EDFM and Viscous grain shearing model using the parameters of Idukki Reservoir from sites 1-3.

the sandy sediments found in the Idukki Reservoir for sites 1-3. It is noted that in the site #1 the compressional velocity is found to be in the range 2300 m/s - 2500 m/s. In the other 2 sites the compressional velocity is found to be in the ranges of 1800-2000 m/s. The SAX99 range of theoretical wave dispersion compressional velocity range for EDFM is 1690-1750 m/s, for GS 1760-1800 m/s and VGS is 1660-1740 m/s. The results indicate that for low porosity the sound speed increases.

4.2 Compressional Attenuation

The compressional attenuation values obtained from sediment data are comparable at sites #2 and site # 3 as shown in the figure below:

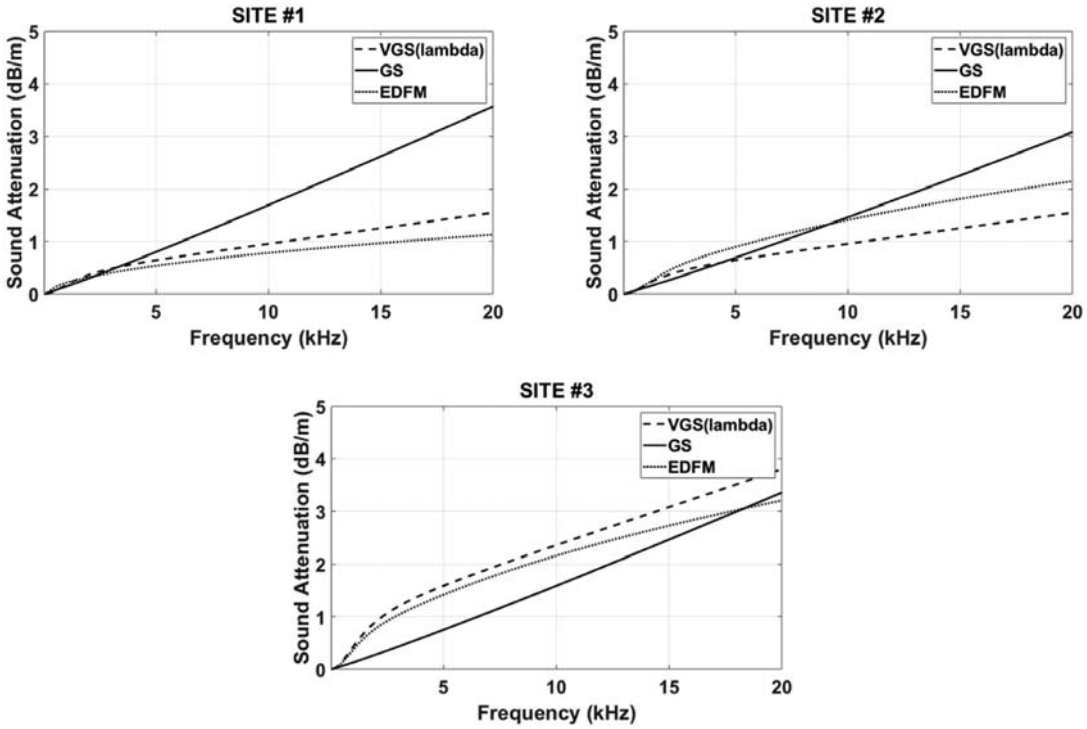

Fig. 5 : The attenuation predicted for Grain shearing model, EDFM and Viscous grain shearing model using the parameters of Idukki Reservoir from site 1-3.

The measured theoretical sound attenuation measured for SAX99 is in the range of 0 to 25 dB/m. At site # 1, the attenuation values are considerably lower as the sediment is denser and less porous. Results show that attenuation increases linearly with increase in frequency[10]. The attenuation predicted by the EDFM is slightly lower at very low frequencies. The attenuation values are closer to 0.25 dB/m/kHz, which is typical of coarse sandy sediments.

5. CONCLUSION

The wave properties of the sediments collected from Idukki reservoir is analysed using EDFM, G-S and VGS models. These theoretically modelled predictions are compared with the measured wave properties of field observation data from SAX99. The sediments from site #1 are found to be harder and highly consolidated and are sandy gravel in texture. The site #2 and site #3 sediments are found to be almost similar in composition. They are observed to be gravelly very fine medium sand. The porosity of site #1 is 0.133 which is lesser compared to site #2 and site #3 which has porosity of 0.52667 and 1.123 respectively.

The compressional velocity predicted for grain shearing model, EDFM and viscous grain shearing model ranges between 2300 m/s to 2500 m/s for site #1 and for site #2 and site # 3 is between 1800 m/s to 2000 m/s. The compressional velocity of site #1 is higher possibly due to lesser porosity. The geoacoustical parameter i.e. the compressional velocity mainly is observed to be highly correlated to the porosity and bulk density than the mean grain size. The compressional attenuation predicted for grain shearing model, EDFM and viscous grain shearing model predicts an attenuation range between 1 dB/(m.kHz) - 3 dB/(m.kHz) for the 3 sites. The attenuation is observed to be high for site #2 and site #3 due to high porosity.

6. ACKNOWLEDGEMENTS

Authors intend to thank Dr. Duvvuri Seshagiri, Director, NPOL for providing facilities of the research and thankful for the funding support of research scholarship No. NPOL/A/EST/127/SRF/JRF.

REFERENCES

[1] M.J. Buckingham, 2005. Compressional and shear wave properties of marine sediments: Comparisons between theory and data, *J. Acoust. Soc. Am.*, **117**(1): 137–152.

[2] T.B. Hefner and K.L. Williams, 2005. Sound speed and attenuation measurements in unconsolidated glass-bead sediments saturated with viscous fluids, *J. Acoust. Soc. Am.*, **120**(5): 2538-2549.

[3] M.A. Biot, 1962. Generalized theory of propagation in porous dissipative media, *J. Acoust. Soc. Am.*, **34:** 1254–1264.

[4] M.J. Buckingham, 2007. On pore fluid viscosity and the wave properties of saturated granular materials including marine sediments, *J. Acoust. Soc. Am.*, **122**(3): 1486–1501.

[5] P. Chotiros, 2017. Acoustics of the seabed as a poroelastic medium, Springer, Berlin.

[6] R.L. Folk and W.C. Ward, 1957. A study in the significance of grain-size parameters of sedimentary petrology, *J. Sediment. Petrol.*, **27**(1): 3–26.

[7] D. Stoll, 1989. Sediment Acoustics, Springer-Verlag, New York.

[8] K. L.Williams, 2001. An effective density fluid model for acoustic propagation in sediments derived from Biot theory. *J. Acoust. Soc. Am.*, **110**(5): 2276–2281.

[9] E.L. Hamilton, 1980. Geoacoustic modeling of the sea floor, *J. Acoust. Soc. Am.*, **68**(5): 1313–1340.

[10] D. R. Jackson and M. D. Richardson, 2007. High-Frequency Seafloor Acoustics. Springer Science and Business Media.

The Journal of Acoustical Society of India : Vol. 52, No. 4, 2025 (pp. 175-182)

Spectral composition assessment of seasonal shallow water sound intensity

Nimmi R Nair[1], Elizabeth Shani N.X.[2] and Anil Kumar K.[3]
[1]Naval Physical and Oceanographic Laboratory, Ministry of Defence, Thrikkakara, Kochi, Kerala-682 021,India.
[2]Centre for the Development of Advanced Computing, (C-DAC), Vellayambalam, Thiruvananthapuram, Kerala-695 033, India.
e-mail: shany.pisces@gmail.com

[Received: 01.09.2025; Revised: 27.10.2025; Accepted: 31.10.2025]

ABSTRACT

Underwater acoustic propagations are controlled by prevailing environmental conditions especially by means of sound speed structure. Accounting these regional conditions causing the propagation variability can improve the performance of various underwater acoustic devices. The present work discusses the propagation loss variability of a shallow station near off Kollam with respect to season and frequency. A numerical acoustic propagation model RAM has been used for simulating this range dependent signal transmission. Two propagation conditions are considered such as shallow to deep (Downslope) and deep to shallow (Upslope). Subsequently, transmission loss corresponds to two major seasons of the region are modeled at lower frequencies such as 150 Hz, 250 Hz, 400 Hz and 600 Hz. Comparing the upslope and downslope geometry reveals that TL values are lower in the downslope than in the upslope. Seasonal variations are more substantial in shallow stations, furthermore this comparison demonstrate that higher frequencies 400 Hz and 600 Hz are detected with low TL during winter due to the presence of surface ducts and inversion layers in February. However, the negative gradient SSP observed in monsoon season cause the rays to refract downwards hence a receiver in deeper depths marks high intensity signals than a shallow receiver in downslope scenario.

1. INTRODUCTION

Predicting the acoustic propagation in complex shallow water environment is challenging due to the substantial spatio-temporal variability[1]. Seasonal oceanographic features alter regional sound speed structures through ocean temperature and salinity[2, 3]. These periodic seasonal conditions control the underwater waveguide characteristics and the subsequent sound propagation[4, 5, 6]. Temporal changes in ocean environment range from diurnal to seasonal scale and hence the waveguide properties; this necessitates the setting up of continuous ocean monitoring networks. Field measurements are extensively used to monitor the seasonal propagation features, however they are intricate to carry due to some practical limitations from natural calamities to the requirement of high power and storage devices. Thus as an alternative underwater acoustic models are emerged and bagged the acceptance in ocean research community for its minimal implementation schemes, reliable performances and broad spatial and temporal coverage[7]. However, these models require adequate sampling of certain ocean parameters and among them sound

speed profile can effectively convey all the medium vicissitudes hence SSP are preferred herein to address the seasonal channel properties[8, 9]. In the current work year-long CTD measurements were carried out to study the regional propagation characteristics using an implemented acoustic model.

2. LOCATION AND DATA

Coastal station near off Kollam has been chosen to explore the complex shallow water propagation characteristics of South Eastern Arabian Sea (SEAS). SEAS witness highly dynamic seasonal patterns that affect the regional acoustic propagation. Here the sound propagation is simulated along a 2D section perpendicular to the shore with bathymetry changes from very shallow 55 m to 975 m deep stations. Study area SEAS is known for its seasonal reversal of winds and currents with the presence of certain oceanographic phenomena. Features like upwelling, downwelling, coastal fronts and internal waves were properly accounted in several studies for its implication on regional sound propagation[10, 11, 12].

As shown in Fig. 1 the study covers the measurement stations which are approximately 7 km apart. Latitude and longitude of the stations are 8.5°N and 76.06°E to 76.73°E respectively. Depends on the bathymetry of the location two types of propagations downslope and upslope are considered respectively as shallow to deep and deep to shallow. In both the conditions acoustic propagation witnesses sudden changes in bathymetry. In downslope the source is at first station of depth 55 m, afterwards station depth increases as 63 m, 72 m, 111 m, 341 m, 595 m and 975 m respectively at 26 km, 37 km, 44 km, 55 km, 62 km and 73 km distance towards the offshore. In upslope source is considered at the deepest station (975 m) and the propagation is towards the shore with decreasing bathymetry.

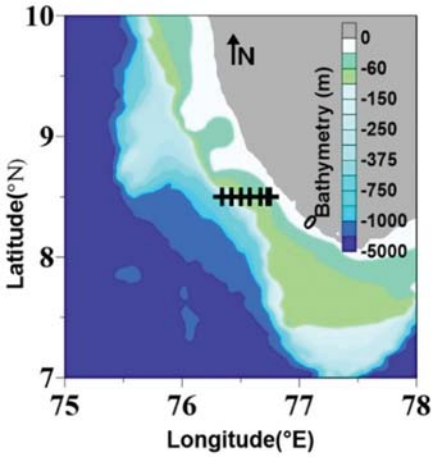

Fig. 1: Location map shows the study area at 8.5^{0}N latitude with 7 measurement stations spanning from to 76.06^{0}E to 76.73^{0}E.

This study utilizes monthly sound speed data from these stations. *In-situ* measurements are carried out on temperature, salinity, bathymetry and bottom properties. Among them, seasonality of the water column was addressed in terms of temperature and salinity considering the other two parameters is invariant.

2.1 Seasonal Sound Speed Profile

Fig. 2 shows the vertical SSP at these seven stations in four months representing two dominating seasons of the region; months January and February as winter, June and July for monsoon. In winter, SSP shows

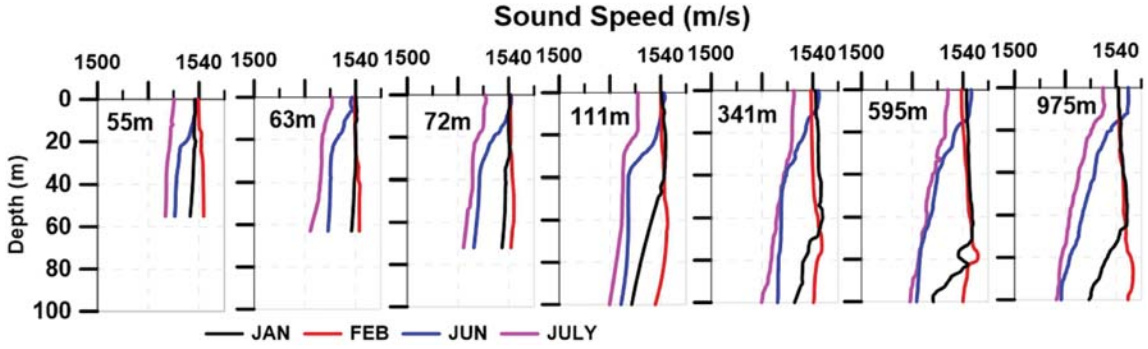

Fig. 2: Sound Speed Profiles up to 100 m depth at seven stations in four months, respective station depths are mentioned in each plot.

surface ducts with the presence of temperature inversion layer in February. However such inversion layers are not observed anywhere in very shallow stations or above 70 m depth in deep stations. Inversion layers have significant role in long range acoustic propagation it offers waveguide effect by continuous reflection at the surface and refraction at layer boundary. Negative sound speed gradient is observed in summer monsoon this cause the sound rays to refract downwards result in repeated bottom interactions and reduces the propagation range. Analyses also points out that, the seasonal variations in SSPs are prominent at both shallow and deep stations. This seasonality is found to affects the entire water column and is more affected at the thermocline regions; above this layer in the upper few meters (10-20 m) monthly profiles are nearly comparable. Subsequent sections discuss the impact of these observed sound speed variability on Transmission Loss (TL).

3. METHODOLOGY

Study addresses the variations in regional propagation characteristics arise from seasonal sound speed profiles and bathymetric variations on selected frequencies. Acoustic waveguide features of SEAS are explored by means of transmission loss computed using an appropriate acoustic propagation model-RAM. Model execution has been carried out in selected months at four frequencies such as 150 Hz, 250 Hz, 400 Hz and 600 Hz. Spectral comparison of TL facilitated the selection of optimum frequencies which supports minimum propagation loss. Furthermore TL variability with respect to upslope and downslope condition analyzed the various propagation paths that appeared in each scenario. Model domain consists of both water column and sediment layer in vertical and 80 km horizontal range between the source and receiver.

3.1 Model Implementation

PE (Parabolic Equation) models are known for its competence to solve range-dependent, low frequency underwater acoustic propagations. They resolve the acoustic propagation through range marching solution; sound field at a certain range is used to fetch the next range without explicitly solving the depth-separated Helmholtz equation. Inherently PE models have limitation regarding the angle of propagation imposed by the paraxial approximation however recent developments results in wide-angle capability makes it suitable for handling range dependent depth varying propagation problems[13].

Among the various PE approaches, RAM (Range dependent Acoustic Model) is widely used for long range low frequency scenarios[14]. RAM follows the numerical solution of PE based on split-step Pade´ solution known for the most efficient numerical scheme. This model allows the user a trade-off between the angular range and computational efficiency, by choosing the number of terms to be used in Pade´ approximation. In RAM, the paraxial approximation is relaxed to a great extent and chosen wider angular range resulting from more number of terms in Pade´ approximation. However PE models have restricted use in certain simulations that involves steeper angles. Starting field is as a self-starter based on PE method[15].

To accommodate the prevailing propagation environment, the field observations at regular range intervals have been inputted in the model. Key factor considered to include the seasonality is the sound speed as discussed in sect.2.1. Furthermore, the bathymetric variations and bottom parameters such as compressional speed (m / s), compressional attenuation coefficient (dB/λ) and density (g / cc) are also included in the model at fixed horizontal ranges. Model generates the TL values corresponding to the given environment and frequency in a uniform range-depth grids.

4. RESULT AND DISCUSSION

The environmental conditions that support minimum propagation loss particularly in low frequency spectra are discussed. Propagation characteristics of the selected location has simulated in terms of TL. Fig. 3 shows TL curves corresponds to downslope (solid line) and upslope (dotted line) with respect to month and frequency, while Fig. 4 shows 2D-TL mosaic. The source and receiver depths were fixed respectively at 20 m and 50 m. In Fig. 3, x-axis denotes the horizontal propagation range in km and y-axis is the computed TL

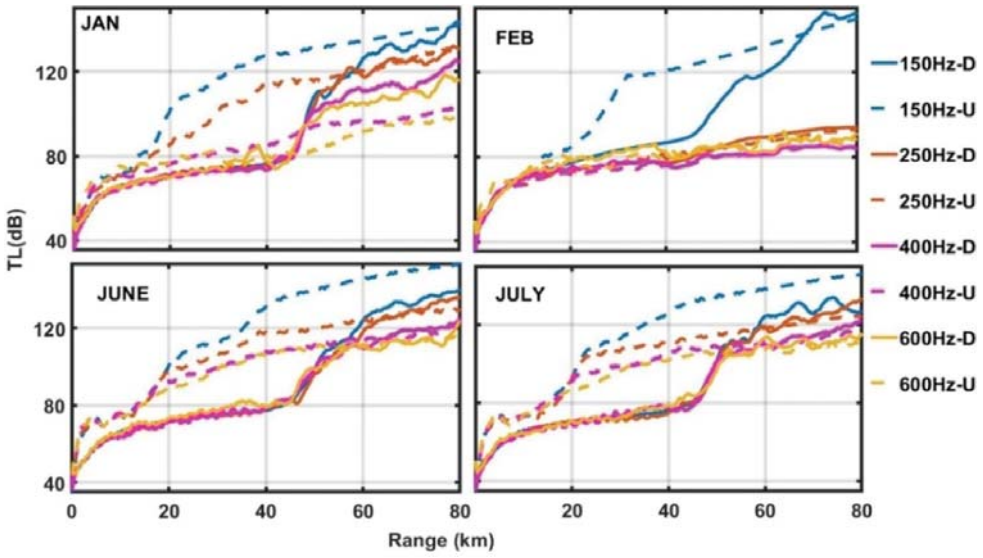

Fig. 3: Monthly TL curves of Leg1 with SD=20 m, RD=50 m and range 80 km at four frequencies in downslope (solid line) and upslope (dotted line) cases.

in dB. Typically when range increases transmission loss also increases therefore as signal forward its intensity got reduces and after particular range the detection ceases to zero. Higher TL values indicate the more propagation loss and hence the shorter signal ranges. Even though the model simulation has been extended to 80km the corresponding TL values are much higher and only in selected conditions the signal propagates with detectable TL level. As seen in figure, below 10 km TL curves have steep slope similar in both upslope and downslope, after that curves maintain a uniform slope up to 50 km. In this mid-range propagation, TL values are low in downslope than upslope. At farthest ranges beyond 45km, the TL values in downslope begin to increase and equals with that of upslope this agrees the high transmission loss across all frequencies.

Observations show that TL values show significant variations with respect to frequency as well. This frequency dependent disparity in TL has been comprehensively addressed in this study. However the spectral variations in TL are found to be dissimilar in upslope and downslope. In upslope, the spectral dissimilarities are prominent beyond 15 km range. For instance lower frequencies 150 Hz and 250 Hz have high TL value than 400 Hz and 600 Hz. However the downslope TL curves keep low spectral variability and the dispersion effects are significant merely after 50-55 km.

Seasonal analysis shows that winter season (January and February) corresponds to lowest TL value especially in February. During this month TL curves are comparable across the frequencies in both upslope and downslope, except 150 Hz which shows increased TL level. Analysis shows that in February SSP have inversion layers[16] around 80m depth which supports the ducted propagation and resulted in minimal TL level. This observation is very relevant in the context of examining the seasonal changes in regional propagation characteristics. Winter months are favorable for extended signal detection range especially in downslope scenario, however the noise levels has to be considered. This observation also proposes the existence of optimum frequency as 400Hz which have the lowest TL of all other frequencies considered here. Importance of surface ducts in underwater acoustic propagation is detailed in next section.

Surface duct continuously enhance the acoustic waves intensity due to low attenuation and long range propagation through the surface channel. This propagation is featured as the repeated surface reflections at the surface and refractions at the lower layer boundary correspond to the maximum of sound speed. However the ducted propagation is limited by waveguide cut-off frequency and this can be determined from duct thickness and the sound speed gradient[17]. The cut-off frequencies are 350 Hz and 410 Hz

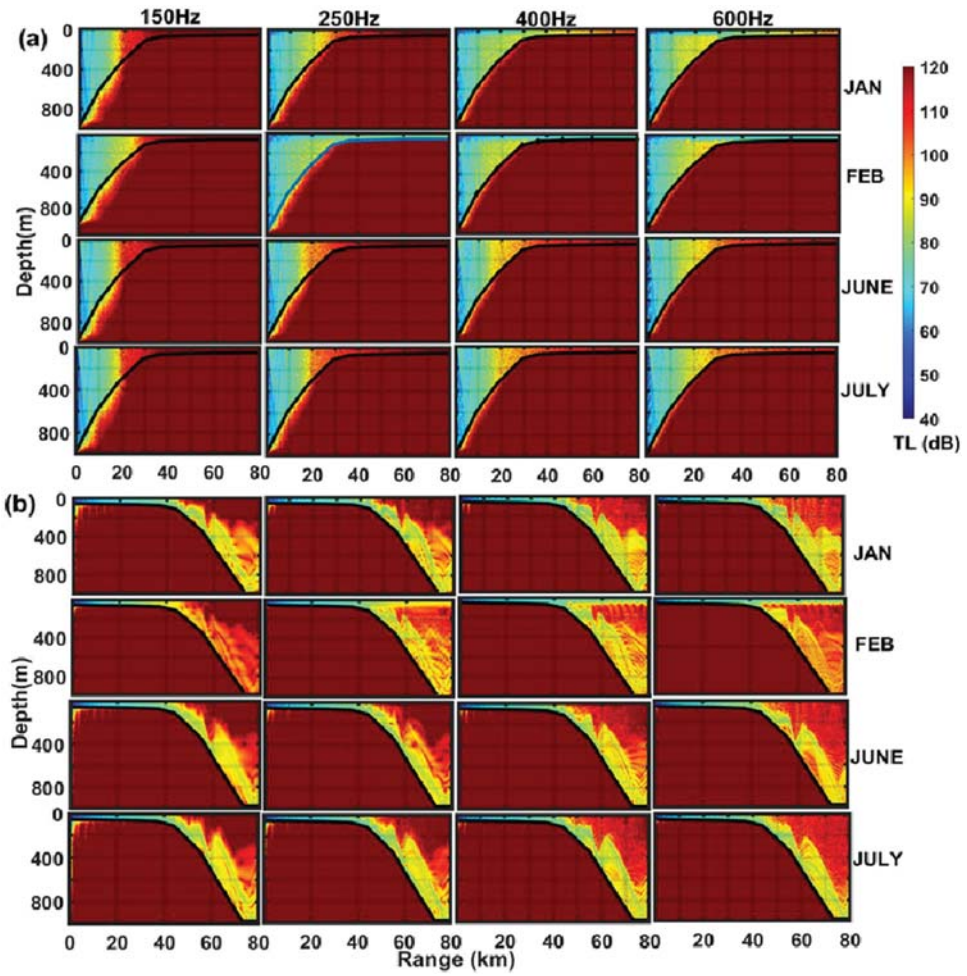

Fig. 4: TL Mosaic of Leg1 at four selected months and frequencies in (a) upslope and (b) downslope propagation conditions.

respectively in upslope and downslope in January, however in February it is 199 Hz in upslope this results in ducted propagation from 250 Hz onwards. Surface duct doesn't support the signals that are below its cut off frequency hence the signals at frequency 150 Hz will not be get ducted and this explains the observed minimal seasonal variations at 150 Hz.

In June and July the corresponding SSPs are not supportive of ducted propagation and hence the TL values are higher than the winter in both the cases. However a common observation that can be made from these typical seasonal profiles is TL always has low value at 400 Hz compared with other three frequencies. This put forward the concept of optimum frequency which arises due to the combination of high bottom penetration at low frequency and increased volume scattering at high frequencies. These two processes concurrently mark out the optimum frequency for the given environment, bathymetry and the propagation condition which exhibits low TL values among the selected frequencies.

It can be observed from the Fig. 3 that downslope propagation is susceptible to high transmission loss at the farthest ranges. Since the propagation beyond the initial shallow ranges is mostly bottom bounded and this marks weaker signals at 50 m. However Fig. 4 shows that deeper depths receive intense signals improving the SNR for signal detection. This analysis highlights the importance of source receiver geometry in describing signal characteristics.

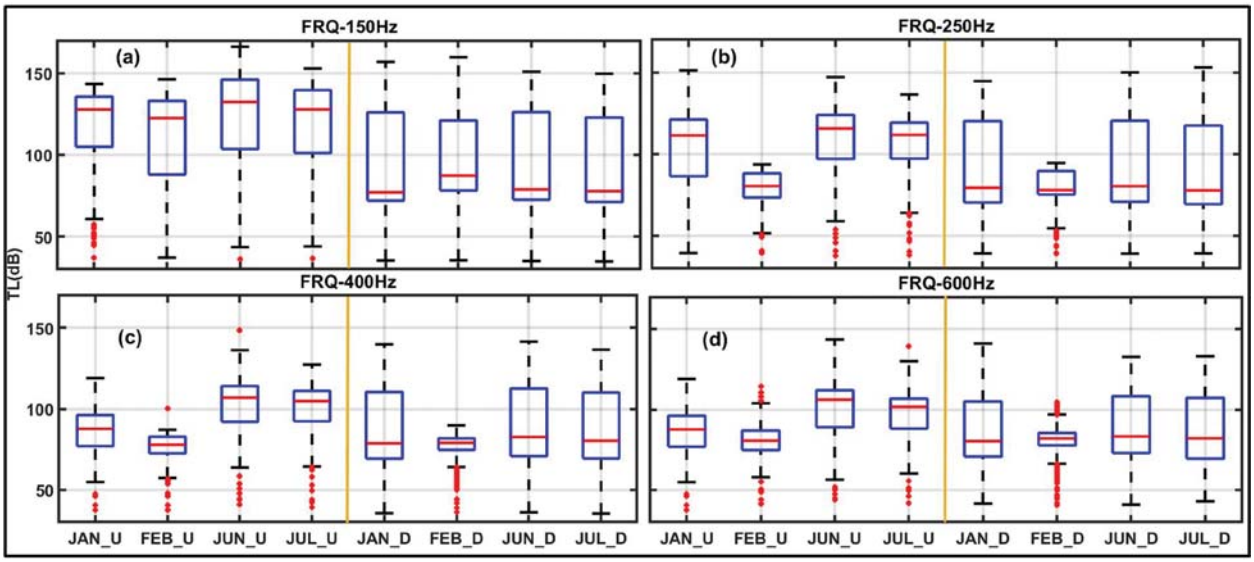

Fig. 5: Boxplot with respect to frequencies 150, 250, 400 and 600Hz in upslope (U) and downslope (D), at January (JAN), February (FEB), June (JUN) and July (JUL) months.

Fig. 5 gives the boxplot representations of the TL at these frequencies and in each plot, first four left side boxes corresponds to upslope with respect to months and similarly right side last four boxes represents the downslope. The boxes denote the model simulated TL values for the whole propagation distance, with 100m range step, up to 80 km from the source point. Analysis shows that seasonality plays a significant role in the pattern and IQR (Interquartile Range) of higher frequencies from 250-600 Hz. At these frequencies, the upslope boxes are observed with short IQR and large numbers of outliers. This implies, distribution follows a steady pattern with significant number of extreme cases on the low TL side. This observation supports long range propagation with minimal signal attenuation and amongst the February have lowest TL level. However the downslope boxes present a different situation with large IQR and no outliers. Yet their February boxes are almost similar with shortest IQR and vast number of outliers. This suggests that lower propagation losses are detected consistently in February month across all the frequencies above the cut-off.

At lower frequency 150 Hz, Fig. 5 (a), seasonal influence is nominal that all the boxes are stretched with large IQR and fewer outliers. Thus the distribution is widely spread and less predictable compared to other frequencies. However less number of outliers indicates that extreme cases are unlikely to occur. At 150 Hz the mean value of the upslope boxes are on the higher side around 130dB compared to downslope which have the mean line at 80 dB. Hence it can be comprehended that without any seasonal differences the upslope have high transmission loss compared to downslope.

5. CONCLUSION

This study addressed the propagation characteristics of Eastern Arabian Sea by means of field measurements and modeling. Sound speed measured from the shallow and deep stations showed significant seasonal variability. Winter months exhibits surface ducts whereas negative gradient profiles were noticed in summer monsoon. Seasonal variations were more prominent at higher frequencies and it is observed that during winter the propagation is enhanced through surface ducts and results in extended signal transmission range. Additionally the propagation is limited by cut-off frequency and found that frequencies 400 Hz and 600 Hz are able to get ducted and lower frequencies are failed to cop up. Thus the spectral variations in TL curves are more in winter time than the other profiles. However this transmission range indicates the lower

TL values and not the signal detection. In a system performance aspect, low TL should be considered along with the ambient noise level in each of the season as discussed in earlier publication[18].

Comparison of upslope and downslope propagation shows that downslope have low transmission loss compared to the upslope. In upslope, the propagation is featured through bottom and surface reflected paths and thus sound energy illuminates the entire water column during the initial ranges. As it propagate further continuous bottom interaction causes the high attenuation loss and signal got diminished rapidly making it unable to reach up to the specific receiver location. In downslope case, propagation is advanced through bottom reflection and refraction at layer boundaries; this confines the rays to deeper depths inhibiting them to travels further upward. Hence a receiver placed in deeper depths receives high intensity than a shallow receiver in downslope scenario.

Analysis using boxplots suggests that frequencies above the cut off follow a regular pattern in upslope, with large number of outliers whereas in downslope the distribution is widely spread and less predictable excluding February. Thus the work analyzed spectral variations in regional waveguide features by selecting the two different climatic conditions-summer and monsoon season of the region. This study can be further extended to deeper locations, accounting further prominent seasons and also other modeling concepts.

ACKNOWLEDGMENT

Authors would like to thank the Director, Naval Physical and Oceanographic Laboratory (NPOL) for the support in the conduct of the study.

REFERENCES

[1] X. Zhang, C. Cheng and X. Han, 2016. Acoustics Propagation properties in the seasonal change environment of shallow sea area, *IEEE/OES China Ocean Acoustics,* pp. 1-5.

[2] S. Khan, Y. Song, J. Huang and S. Piao, 2021. Analysis of Underwater Acoustic Propagation under the Influence of Mesoscale Ocean Vortices, *J. Mar. Sci. Eng.,* **9**(799). https://doi.org/10.3390/jmse9080799.

[3] K. Srinivasu, M.C. Sanjana, G. Latha, T.V.S. Udayabhaskar, H. Rahaman, A. Thirunavukkarasu and R. Venkatesan, 2024. Study on acoustic variability affected by upper ocean dynamics in south eastern Arabian Sea, *Earth and Space Science,* **11:** e2023EA003497. https://doi. org/10.1029/2023EA003497.

[4] A. Affatati, C. Scaini and S. Salon, 2022. Ocean sound propagation in a changing climate: Global sound speed changes and identification of acoustic hotspots, *Earth's Future,* **10:** e2021EF002099. https://doi. org/10.1029/2021EF002099

[5] C. Chen, F. Yan, T. Jin and Z. Zho, 2019. Effect of Eddy on acoustic propagation from the surface duct perspective, *Appl. Acou.,* **150:** 190-197.

[6] S. Wu, Z. Li, J. Qin, M. Wang and W. Li, 2022. The Effects of Sound Speed Profile to the Convergence Zone in Deep Water, *J. Mar. Sci., Eng.* **10**(424). https://doi.org/10.3390/ jmse10030424.

[7] C. Erbe and J.A. Thomas, 2022. Exploring Animal Behavior Through Sound: **1:** Springer Nature Switzerland, ISBN 978-3-030-97540-1, https://doi.org/10.1007/978-3-030-97540-1

[8] S.N.X. Elizabeth, R.N. Nimmi, R.P. Raju and R. Sajeev, 2023. Statistical Study on shallow water soundscape variability of Eastern Arabian Sea using noise level metrics, *Environ. Monit. Assess.,* **195:** 1314, https://doi.org/10.1007/s10661-023-11912-4.

[9] S.I. Siddiqui and H. Dong, 2019. Effects of Water Column Variations on Sound Propagation and Underwater Acoustic Communications, Sensors, **19**(2105), doi:10.3390/s19092105.

[10] R.N. Nimmi, K. Anilkumar and N. Mohankumar, 2015. Quantifcation of acoustic variability from thermohaline felds in the Arabian Sea, International conference on water resources, coastal and ocean

engineering (ICWRCOE 2015), *Aquatic Procedia,* **4:** 466–472

[11] P.V. Hareeshkumar and K.G. Radhakrishnan, 2010. Transmission loss variability associated with upwelling and downwelling of the southwest coast of India, *Def. Sci. J.,* **60:** 476–482.

[12] K.V. Sanilkumar, P.V. Hareeshkumar and K.G. Radhakrishnan, 2002. Oceanographic features and their infuence on acoustic propagation: case studies, *Proceedings of ICONS-International conference on sonar-sensors and systems,* pp. 577-582.

[13] F.B. Jensen, W.A. Kuperman, M.B. Porter and H. Schmidt, 2011. Computational ocean acoustics. Ed. 2. Springer, New York, pp. 476-536.

[14] M.D. Collins, 1993. A split-step Pad´e solution for the parabolic equation method. *J. Acoust. Soc. Am.,* **93:** 1736–1742.

[15] M. D. Collins, 1992. A self-starter for the parabolic equation method. *J. Acoust. Soc. Am.,* **92:** 2069–2074.

[16] P. Thadathil and A. K. Gosh, 1992. Surface layer temperature inversion in the Arabian Sea during winter, *Journal of Oceanography*, **48:** 293–304. https: / / doi.org / 10.1007 / BF02233989.

[17] S. Neethu S. Satheeshkumar, 2018. Problems Related to Acoustic Modelling Using PE Models in Surface Duct Environments, Proceedings of International Conference on Sonar Systems and Sensors, ICONS-2018, India.

[18] S.N.X. Elizabeth, R.N. Nimmi, R.P. Raju and R. Sajeev, 2022. Experimental study on the impact of seasonal sound speed variability on signal detection range in Arabian Sea. Def.Sci.J., **72**(4): 647–653. https: / / doi.org / 10.14429 / dsj.72.17756.

The Journal of Acoustical Society of India : Vol. 52, No. 4, 2025 (pp. 183-190)

An indigenous very low frequency electromagnetic projector-survey, design and performance evaluation

Balamurugan S., V. Vinothkrishnan, Rahul P. Krishnan, Mantu Sahu and Satheeshkumar O.B.

[1]*Naval Physical & Oceanographic Laboratory, Kochi-682 021, India*

e-mail: balamuruganng892@rediffmail.com

[Received: 01.09.2025; Revised: 28.10.2025; Accepted: 31.10.2025]

ABSTRACT

Very Low Frequency (< 500 Hz) sound generation in underwater has wide range of civilian and defence applications. Conventional Piezoelectric Transducers will not meet the sound pressure level requirements as the required displacement is higher. There are other sources like Hydraulic, Pneumatic, and Electromagnetic drives to generate low frequency sound. In this paper indigenous low frequency transducer designs and its limitations are explored. Further a low frequency transducer with a piston driven by an Electromagnetic Shaker was designed, analyzed, fabricated and tested at Acoustic tank and Lake. A sound pressure level of 120-150 dB was achieved in the frequency band of 50-1000 Hz. Also, the effect of hydrostatic pressure on piston was measured at an Anechoic tank with application of different hydrostatic pressure. A power amplifier was designed to drive this transducer in the frequency band of 10 Hz to 1000 Hz, coupled and tested further. Another design with a piston driving a diaphragm was made and its performance was measured. For higher force rating a bigger transducer with piston and oil filled diaphragm was designed with pressure compensation mechanism and modelled using COMSOL. The variation of performance with respect to different parameters were further discussed in this paper.

1. INTRODUCTION

Naval applications of underwater sound generation require a transducer to make the communication between two submerged submarines, in which a projector to transmit the sound and a hydrophone to receive sound on each submarine, the echo ranging requires a projector and a hydrophone usually on the same ship[1]. The useful spectrum of underwater sound extends from about 1 Hz to over 1 MHz with most applications in large bodies of water for example the acoustic communication over thousands of kilometres is possible in the oceans but frequencies below 100 Hz are required because of absorption losses. The frequencies below 100 Hz called very low frequency can be projected by using the Moving coil, Hydrodynamic and electromagnetic transducers[2]. The moving coil type electromagnetic transducer provides very low-frequency sound source in a fairly small package and sound energy down to a few Hertz and other benefit of the moving coil transducers are in very broad-band sound transmissions[3]. Mostly sound projectors for underwater use are resonant high efficiency systems for radiating high intensities over a limited-frequency range. The navy needs broad-band high-fidelity underwater sound sources that produce constant sound pressure over wide-frequency ranges for calibrating standard transducers and for other measurement functions[4]. UW350, compact pressure compensated hydro- sounder with a moving coil vibration exciter wide operating frequency

band extending down to 20 Hz, used for SONAR testing and evaluation, low frequency machine noise simulation and hydrophone calibrations[5]. The principle of the moving-coil electroacoustic transducer is that the coil applied with an alternating current signal is forced to vibrate in the magnetic field to cause the vibration in diaphragm to generate the sound waves in water[6]. The hydrodynamic transducer with siren mechanism used for sound production in water. In this transducer the siren works as a powerful, broadband, less power consumption and produces better acoustic efficiency[7]. The low-frequency sound source of high acoustic output hydrodynamic type projector has been configured to operate over distinct frequency bands, with a bandwidth of approximately 0.4 times of each band-center frequency[8]. For low frequency operation, the structure of the transducer must be large and the underwater acoustic wave projector should be characterized by resonant, efficient, omnidirectional, capable of radiating high power at low audio frequencies, capable of continuous wave or pulse operation, structurally simple, rugged, economical to fabricate and operate and comparatively small relative to its power capacity[9]. The electroacoustic transducer with a vibratile plate member driven by electromagnetic forces generated in an air gap maintained between an inertial mass structure and the vibratile plate member is a high-power, low-frequency transducer designed for high efficiency operation[10]. In this paper one such design is being developed to operate in the very low frequency band with broad band characteristics. A piston in water driven by low frequency transducer which in turn driven by a power amplifier is fabricated and experimented. Further diaphragm design was made and evaluated. The design of higher force rating is proposed.

2. INDIGENOUS IN-HOUSE LOW FREQUENCY TRANSDUCERS

A low frequency mechanical noise generator shown in (Figure 1) with a circular array of pipes each with different diameter and length tuned for different frequency to cover the band of 10 Hz to 300 Hz which is excited by individual hammers[11]. The response of the transducer is shown in (Figure 2) where the levels are in the order of 110 to 140 dB. The shortcoming of this type of transducer is the levels are not customizable and

a: Array of Pipes **b:** Impact hammers **c:** Transducer assembly

Fig. 1: Mechanical Noise Generator

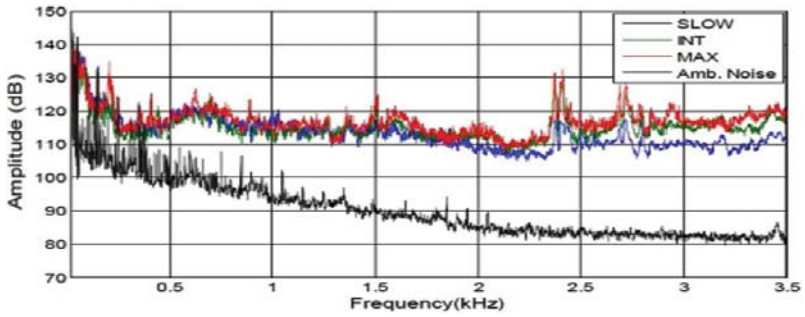

Fig. 2: SPL of Mechanical Noise Generator at different speeds

size is too big for the SPL being produced. A low frequency multiport tube projector is shown in (Figure 3.a) where the transducer has resonance around 1000 Hz and frequency band of 100-3000 Hz. The maximum SPL it can produce is 188 dB at 1 kHz. The weight of the transducer is 250 kg and at below 500Hz frequency the SPL levels are low for this transducer[12]. A flex-tensional transducer (Figure 3.b) with shell resonance around 1.5 kHz driven by PZT stack has relatively better performance at low frequency however at very low frequency below 300Hz the achieved sound pressure levels are lower and around 120 - 130dB[13]. The Free Flooded ring transducer is shown in (Figure 3.c) where the response is higher from 500 Hz onwards however below 500 Hz similar to flextensional transducer the performance is limited[14].

a: Multi Port Tube Projector

b: Flextensional Transducer

c: Free Flooded Ring Transducer

Fig. 3: Low Frequency Transducers

3. VERY LOW FREQUENCY ELECTROMAGNETIC PROJECTOR

A Very Low Frequency Electromagnetic transducer was designed where the driving mechanism is an electromagnetic coil assembly. A B&K Type 4809 45 N force rating shaker was used as the driving mechanism. Two types of designs were considered where one is piston directly interacting with water medium and in another the piston is coupled to a diaphragm and the diaphragm interacts with the water medium (Figure 4).

When piston directly interacts with water medium the challenge is to achieve sealing between piston rod and the enclosure. In second case the diaphragm acts as sealing for the driving mechanism from water.

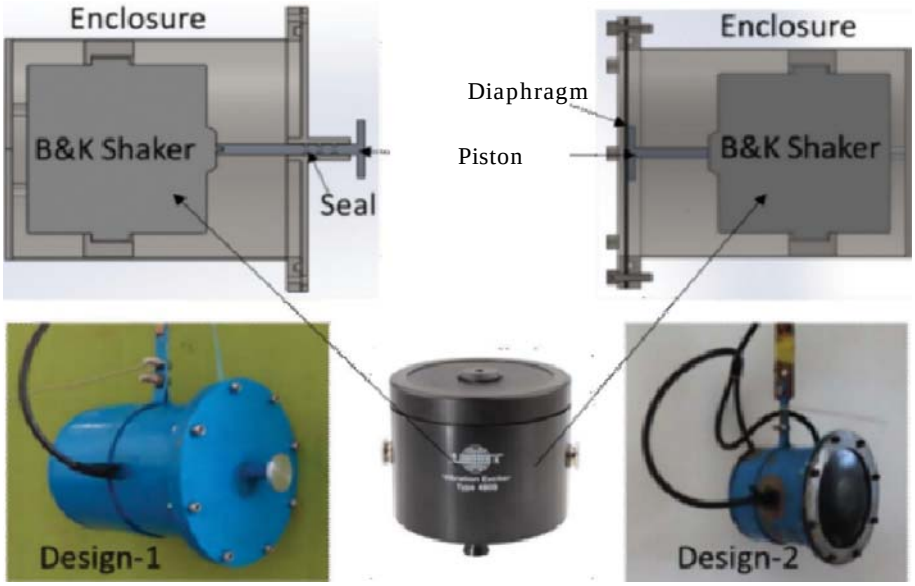

Fig. 4: Design-1 and Design-2 of Very Low Frequency Transducer

3.1 Piston, Diaphragm and Enclosure

The far field axial pressure generated by a baffled circular piston is given by,

$$P(r) = (1/2)\,\rho\, c\, U\, (a/r)\, ka$$

Where, ρ - density of the medium, c - sound speed in the medium, U - magnitude of the displacement of the piston, a -radius of the piston, r - distance from source and k - wave number[15]. Considering the force rating of the B&K shaker and to achieve maximum SPL a piston of 50 mm diameter with lighter material i.e. Aluminium was taken. The frequency band of interest is 50-1000 Hz. For inserting rod seals, the grooves were provided for piston in design-1 with longer piston rod which was coupled with shaker head. For design-2 piston is made without grooves and shorter rod where the piston radiating face is pasted with the rubber diaphragm. The diaphragm was designed and moulded with Styrene Butadiene Rubber (SBR) material in compression moulding machine with proper mould, which was attached to the enclosure by means of fasteners. This diaphragm is driven by piston connected with exciter during underwater sound generation. The enclosure was designed to withstand a pressure of 20 bar and provision was given to take the connections out through cable. In design-2 a passive pressure compensation was provided by fitting a pneumatic valve where compressed air was filled inside the enclosure for diaphragm to withstand the external pressure. The enclosure was fabricated in mild steel and two types of lids were made for two designs. In design-1 the lid is sealed against enclosure using O – rings and a sleeve is provided in middle to accommodate piston rod with seals. In design-2 the lid is in form of ring which will arrest the diaphragm against the enclosure. Overall weight of transducer in both the designs is less than 15 kg.

3.2 Power Amplifier

Power amplifiers play a crucial role in boosting low-power input signals to higher power levels, allowing various devices to operate effectively in a wide range of applications. They are generally classified into linear and switched-mode types, each suited to different operational needs. For driving an electromagnetic load between 50 Hz and 1 kHz, with a power requirement of up to 75 VA and a maximum current of 5 A, linear power amplifier was chosen over a switched-mode since it offers following advantages. Linear amplifiers ensure the output signal closely matches the input without distortion, which is essential for preventing unwanted harmonics and potential mechanical resonance in electromagnetic loads. It offers a flat frequency response, providing consistent performance across a wide range of frequencies, which is crucial for maintaining stability from 50 Hz to 1 kHz.

3.2.1 Design

The amplifier was designed with two power op-amps (PA 05) arranged in bridge tied load configuration as shown in (Figure 5). The output can drive reactive loads and was coupled to the load through an impedance matching transformer. The amplifier can mute or un-mute through TTL control. The output of the amplifier was designed to deliver a maximum power of 100 VA. Distortion level would be of the order of less than 1% at full load. Amplifier has built-in overload / fold over current and over temperature protection. The power op-

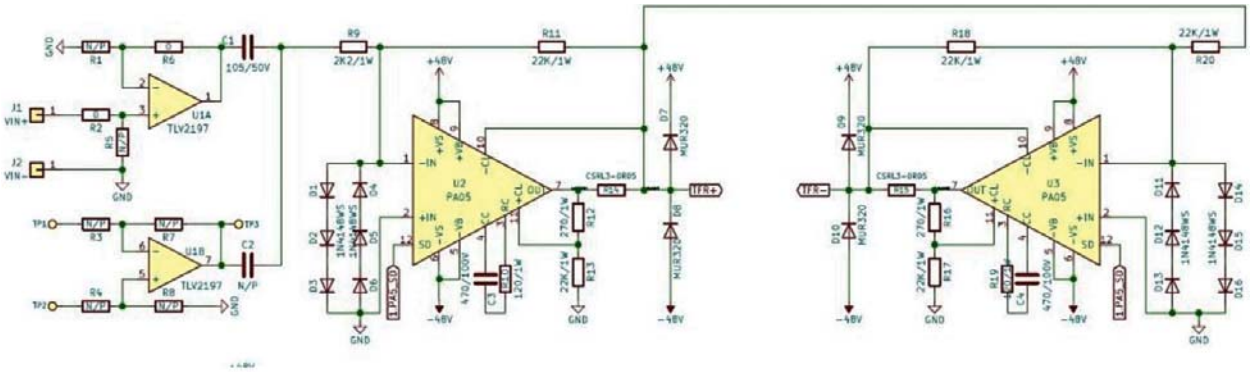

Fig. 5: Schematic of Power Amplifier Design

amps used were class AB linear with MOSFET output stage. Both master and slave were inverting power opamp with a voltage gain of 10.

3.2.2 Development and Results

To evaluate the performance of the power amplifier, a simulation model was initially created using LT Spice. This simulation helped analyze the transient response of the amplifier circuit from 50 Hz to 1 kHz, which were the critical frequencies for the application. The transient response analysis revealed how the amplifier behaves with time-varying signals, ensuring that it can accurately reproduce the input signal without distortion at these frequencies. (Figure 6 and Figure 7).

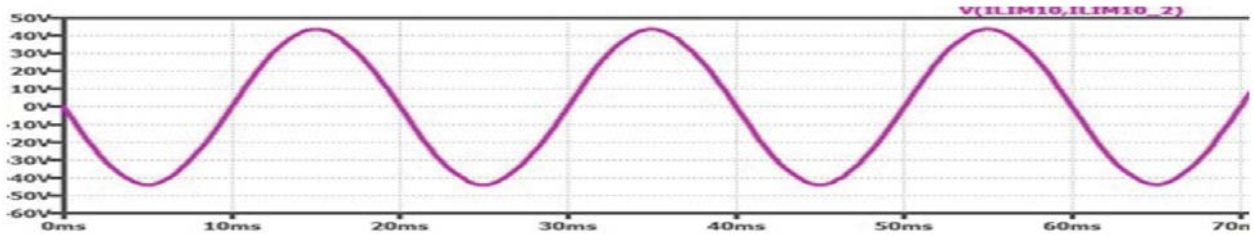

Fig. 6: Transient Response of Power Amplifier (50Hz, 15Ù Resistive Load)

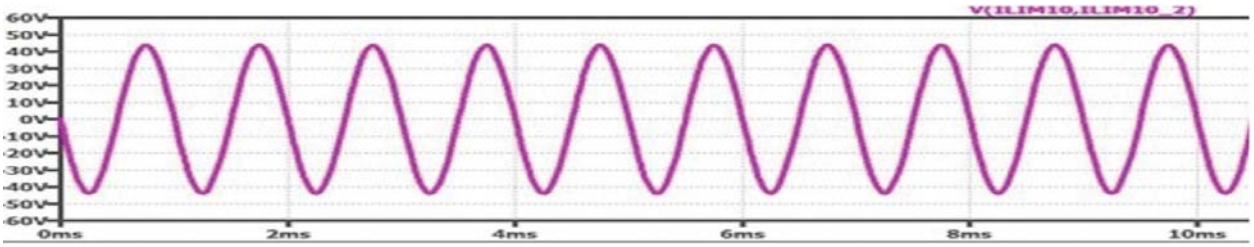

Fig. 7: Transient Response of Power Amplifier (1kHz, 15Ù Resistive Load)

Additionally, a frequency response analysis was conducted to assess the amplifier's gain stability across the desired bandwidth. The results demonstrated a consistent gain from 50 Hz to 1 kHz (Figure 8), indicating that the amplifier can maintain uniform performance over this range, which is essential for driving electromechanical loads effectively.

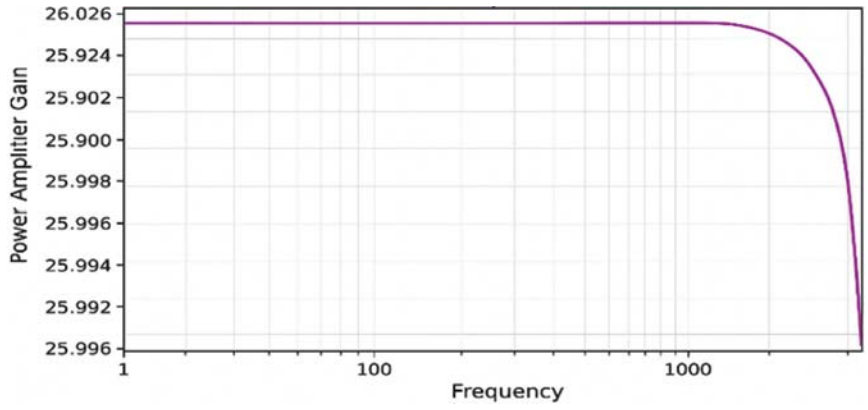

Fig. 8: Magnitude plot of Frequency Response of power amplifier

The simulation, a prototype for bench testing (Figure 9) was developed. The physical prototype was constructed to validate the simulation results in a real-world scenario. Prototype was interfaced and tested with low frequency electromagnetic projector and validated the results with experiments.

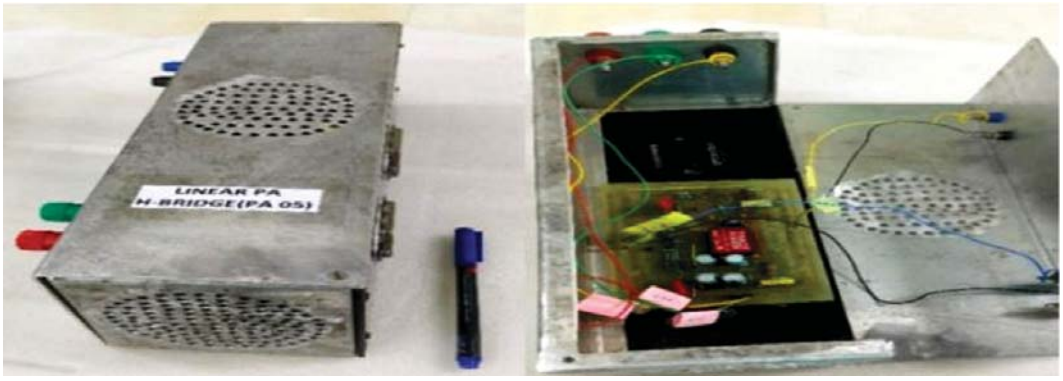

Fig. 9: Lab level prototype of Power amplifier

3.3 Experiments

The transducer was initially pressure tested in a pressure vessel up to 20 bar as part of qualification. The transducer was lowered to a depth of 6 m at acoustic tank and driven by the power amplifier. At different spot frequencies the sound pressure levels were measured using a standard hydrophone at far field distance. Later an underwater accelerometer was kept at the piston to measure the acceleration along with the sound pressure levels. However, the weight of the accelerometer reduced the SPL levels due to loading in the piston as shown in (Figure 10). The transducer was then taken to a reservoir and sound pressure levels were measured again without reflection. However, at lake the level could not be measured below 300 Hz due to noise levels.

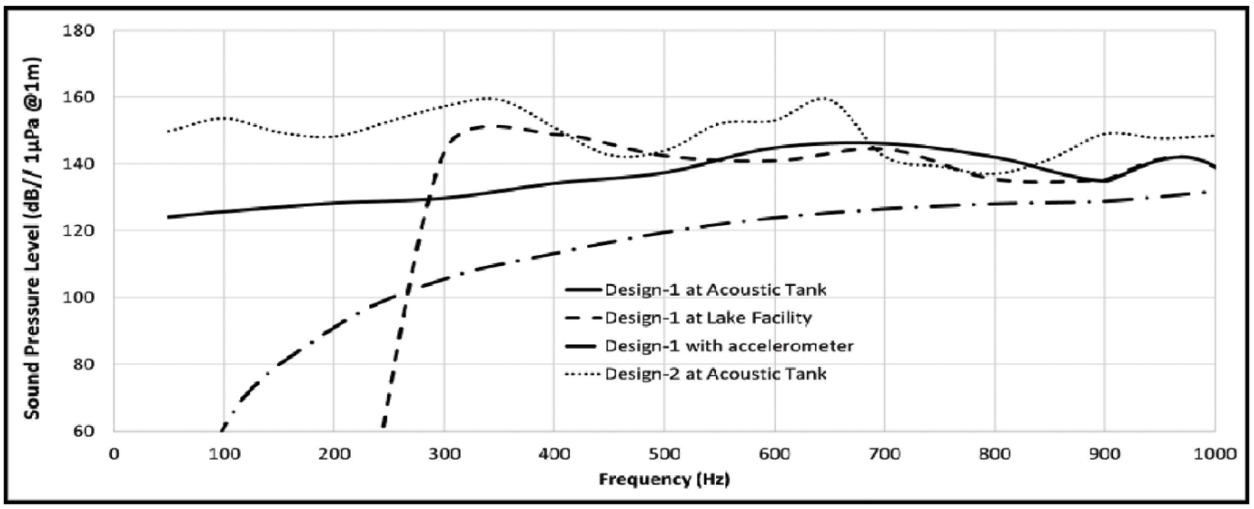

Fig. 10: Sound Pressure Level of Design-1 and Design-2

Overall, the sound pressure level of 120-140 dB was achieved in the frequency band of 50-1000 Hz. The design-2 transducer was lowered at acoustic tank and sound pressure level was measured and around 150 dB was achieved in the frequency band of 50-1000 Hz. To study the effect of hydrostatic loading on piston the Design-1 transducer was lowered at Anechoic water pressure tank where the transducer was excited with fixed current and its acoustic response was measured at different pressures from 0 MPa to 20 MPa and relative variation in pressure was measured and shown in (Figure 11). The results do not show any trend and Anechoic capabilities of tank at low frequencies are limited.

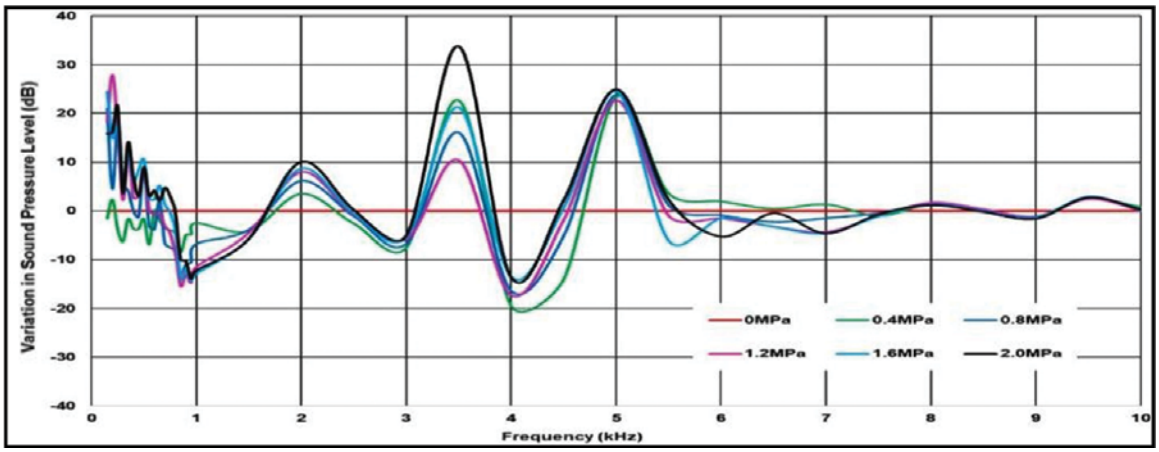

Fig. 11: Variation in SPL w.r.t. Pressure in Design-1

4. HIGHER FORCE ELECTROMAGNETIC PROJECTOR

A new transducer was designed with force rating greater than 100 N using COMSOL. The transducer has a piston and diaphragm where the coupling between the piston and diaphragm is through oil medium shown in (Figure 12.a). To compensate the hydrostatic pressure a bellows is provided which is flooded with water and other side filled with compressed air. The transducer is modelled in COMSOL and the SPL was computed using both analytical method and FEM and the results are shown in (Figure 12.b).

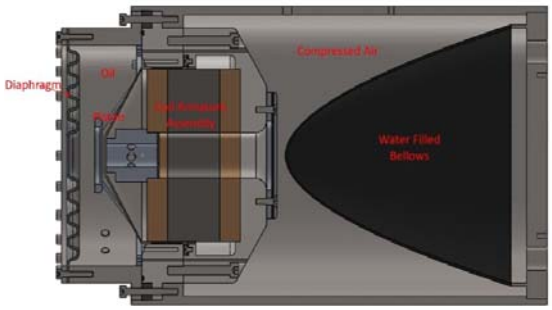

a. Schematic

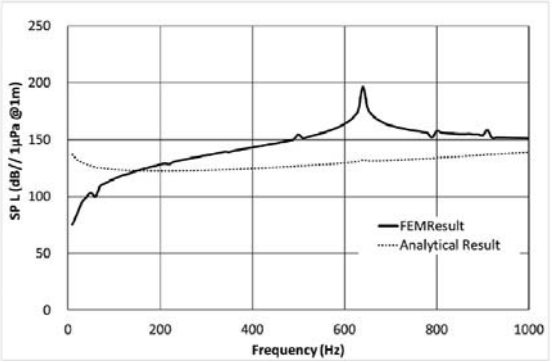

b. Computed SPL

Fig. 12: Higher Force Electromagnetic Projector

5. CONCLUSIONS

In comparison to in-house PNM and PZT based transducers the Electromagnetic based low frequency transducers have better sound pressure level performance at low frequencies, lighter weight and broadband response also. Available B&K electromagnetic shaker was used to drive a piston in two types of design and experiments were conducted with a linear power amplifier. Further a higher force transducer is being designed and its analytical and finite element results were presented.

6. ACKNOWLEDGEMENT

The authors thank Division Head, Transducer Engineering Division, Group Director, Transducer Group for their valuable suggestions and Director, NPOL for providing facilities and encouragement to do the work.

REFERENCE

[1] R.J. Urick, 1983. "Principles of Underwater Sound", 3rd Edition, *Peninsula Publishing, Los Altos Hills, CA*.

[2] Charles H. Sherman, John L. Butler, 2007. "Transducers and Arrays for underwater sound", Third Edition, *Springer Science & Business Media, New York*.

[3] John C. Cochran, 2022. "A Moving Coil Transducers in Introduction to SONAR transducer design", *John Wiley & Sons, Inc.* p. 407.

[4] Claude C Sims, 1959. "High fidelity under water sound transducers, USRL J9", *IRE Proceedings*, **47:** 866-871.

[5] Data Physics Corp," UW350 Underwater acoustic projector", DP-DS-UW350.

[6] "Moving coil electroacoustic transducer", Jianjian Wang from US-Patent No. US 9, 369, 806 B2 Jun. 14, 2016.

[7] S. Yoshikawa and K. Koyano,1995. "Hydrodynamic siren as a broadband underwater sound projector", *JASA*, **98**(2): 1047-1056.

[8] M / s. Hydro Acoustics Inc., USA,"Very low frequency underwater projectors".

[9] "Electromagnetic transducer for underwater low frequency high power use", Frank Massa, Cohasset, Mass. Appl. No.: Filed: 940, 669, Dec. 11, 1986.

[10] Robert H. Mellen and Oild Lyme, 1966. "Underwater Hydrodynamic Acoustic Projector", from US-Patent No. 3, 246, 289.

[11] "Evaluation of Noise Augmentation Unit", UARF DRDO-NPOL-TTM-TER-023- 2015 Date of Issue: 13 Apr 2015.

[12] "Transducer catalogue", Naval Physical and Oceanographic Laboratory,July 22.

[13] "Technology focus", "Defence Research and Development Organisation", **21**(4). August 2013.

[14] "Technology focus", "Defence Research and Development Organisation", **32**(23) May 2024.

[15] Lawrence E. Kinsler, John Wiley & Sons Inc, 2000. "Fundamentals of Acoustics", 4th edition.

The Journal of Acoustical Society of India : Vol. 52, No. 4, 2025 (pp. 191-197)

Optimizing hydrophone performance: a finite element approach to mounting arrangement design

AL Fairooz Sulthan B.A., Sankar G. Nath and Poturaju P. Satyanarayana
Naval Physical & Oceanographic Laboratory, Kochi-682 021, India
e-mail: alphasulthan@outlook.com

[Received: 01.09.2025; Revised: 28.10.2025; Accepted:31.10.2025]

ABSTRACT

Hydrophones are vital tools in underwater acoustic sensing, crucial for applications ranging from oceanographic research to military surveillance. Understanding their performance, particularly concerning the mounting arrangements is essential for accurate data collection especially when it comes to acceleration sensitivity. Acceleration sensitivity is a measure of the response of the hydrophone to platform vibrations. This study investigates the acceleration sensitivity of hydrophone for different mounting configurations. Accurate characterization of hydrophone sensitivity is essential for precise acoustic measurements in various underwater applications. An experimental test is conducted in which the hydrophone is subjected to controlled acceleration while recording its output signal. A finite element model is developed using COMSOL Multiphysics and the results are validated with the measured data. FEM validation confirms the accuracy of the model in predicting acceleration sensitivity. This model is used to simulate hydrophone's response for different mounting setups which include the change in material, change in design and altering the boundary condition. These results indicate that the ear nut mounting configuration amplifies acceleration response levels, particularly at lower frequencies, potentially compromising the hydrophone's acceleration sensitivity. Conversely, eliminating the ears reduced acceleration sensitivity. Additionally, receiving sensitivity measurements are conducted and corresponding Finite Element model is developed. A good correlation between the results is observed. The insights gained from this study contribute to the refining and understanding of the hydrophone's acceleration sensitivity characteristics and provides a foundation to optimize its performance for real world applications. This methodology presented here offers a robust framework for future research and development efforts aimed at enhancing vibro acoustic measurement accuracy and reliability.

1. INTRODUCTION

Underwater acoustics plays a critical role in various marine applications, from oceanographic research to defense applications. At the forefront of this field lies the hydrophone, a transducer that converts sound waves in water into electrical signals. The quest for higher sensitivity and lower noise levels in hydrophones has been a continuous pursuit by scientists and engineers since the early 20th century, with several significant advancements made in electroacoustic transducer design[1].

A major challenge in achieving optimal hydrophone performance is mitigating noise. Hydrophones are susceptible to various noise sources, including background acoustic noise, electrical noise and mechanical noise arising from platform vibrations[1,2]. Among these, mechanical noise often proves to be the most

significant contributor, particularly for towed array hydrophones[1,3]. Minimizing mechanical noise is crucial for enhancing the signal-to-noise ratio (SNR) of a hydrophone. A higher SNR allows the hydrophone to effectively distinguish weak underwater signals from background noise, leading to improved detection capabilities. Additionally, reducing mechanical noise lowers the minimum detectable signal level, enabling the hydrophone to pick up even fainter acoustic signatures[1]. The design of hydrophone mounting arrangement plays a crucial role in this mechanical noise and enhancing the overall sensitivity. This research focuses on Piezo ceramic ring transducers, an active design employed in submarine towed arrays. These hydrophones operate in a dynamic environment where platform vibrations can significantly impact their performance[4,5,6]. A key factor influencing mechanical noise susceptibility in piezo ceramic ring hydrophones is the arrangement in which it is mounted onto the platform to secure them to the towed array structure. The design of hydrophone mounting arrangement plays a crucial role in this mechanical noise and enhancing the overall sensitivity.

In this paper, we present a finite element approach with a particular focus on optimizing the mounting arrangement. Initially an experiment study is conducted with the existing hydrophone where the hydrophone is mounted on a vibration fixture, simulating real-world operating conditions and corresponding voltage response of the hydrophone is measured. The acceleration response in each axis is then calculated and analyzed. This experiment data is used to validate the FEM model developed using commercial FEA software COMSOL MULTIPHYSICS. The validated FEM model is utilized to investigate the effects of different mounting configuration by

- *Change in material:* This is done by introducing titanium nut at mount holes (See Fig. 1b). The inner diameter of the nut is same as the hole diameter of the initial model.
- Modifying the design of hydrophone mounts by using ears made of PVC (See Fig. 1c)
- Altering the boundary condition at the mounting interface. Here, a hydrophone with ears eliminated configuration is studied. (See Fig. 1d). The hydrophone is fixed by inserting its circular edges into a slot in the casing. This ensures that the contact with the casing occurs only along the hydrophone's edges, effectively providing edge-supported boundary condition.

Through these studies, we aim to identify the mounting arrangement that offers the most effective noise mitigation and ultimately leads to superior hydrophone sensitivity performance. The validated FEM model serves as a framework for researchers to explore a wider range of design modifications and boundary conditions beyond the scope of this study.

(a) (b) (c) (d)

Fig. 1: (a) Initial hydrophone model **(b)** Ear nut (varying material property) **(c)** PVC ears (modifying the design of hydrophone mounts) **(d)** Ears eliminated (altering the boundary condition at the mounting interface)

2. ACCELERATION SENSITIVITY MEASUREMENTS

To characterize the acceleration sensitivity of hydrophone and to investigate the mounting configuration, a vibration measurement is conducted. The initial hydrophone(Fig. 1(a)) is mounted onto a vibrating fixture. The fixture is designed such that the fundamental frequency of the fixture lies above the working range of hydrophone to avoid resonance. A vibration shaker is used for the harmonic excitation of hydrophone. The

importance of precisely controlled mounting condition for consistent results was highlighted during experimentation, as the tightness of fasteners used to secure the hydrophone play a significant role in measured response.

During the measurement, the hydrophone is subjected to a harmonic excitation of 1 g along each of its three principal axis (X, Y and Z). The corresponding voltage responses of the hydrophone are recorded[5]. Acceleration sensitivity is a measure of response of the hydrophone to platform vibrations and can be defined as the voltage developed by the hydrophone against acceleration of 1g. It is expressed in dB as

$$AS = 20 \log(\ddot{U}/g) \text{ dB ref 1V/g} \quad (1)$$

Where $\ddot{U}$ is the output voltage developed by the hydrophone, against vibration acceleration of g. The calculated acceleration sensitivities are plotted as a function of frequency to study the hydrophone's response across the desired operating range.

3. ACOUSTIC MEASUREMENTS

To investigate the receiving sensitivity of the hydrophone and compare it with the FEM model predictions, an acoustic measurement is conducted at NPOL's acoustic test facility in the desired frequency band. The hydrophone was cleaned, wetted and soaked for 24hrs before measurement. A projector was placed in the free field of the hydrophone to measure the electrical response of the hydrophone[6]. The measurement was conducted at a set of discrete frequencies relevant to the hydrophone's intended application. At each frequency, the voltage response of the hydrophone was recorded. Receiving sensitivity isdefined as the voltage developed by the transducer when it is placed in an acoustic free field of magnitude 1Pa. It is expressed in dB as.

$$RS = 20 \log(U/P) \text{ dB ref 1V/}\mu\text{Pa} \quad (2)$$

Where U is the output voltage of the hydrophone, against acoustic pressure (P)[1]. The calculated receiving sensitivity is presented as a function of frequency in the results section to visualize the hydrophone's response across the investigated frequency range.

4. FEM MODEL

To perform extended research on hydrophone's performance and complement the experimental findings, a finite element model (FEM) of the hydrophone is developed using COMSOL MULTIPHYSICS 6.1. The geometry of the hydrophone model is created using SOLIDWORKS based on the hydrophone's technical specifications. For the acoustic analysis, infinite water domain is modelled on all sides of the hydrophone and is truncated using perfectly matched layers (PML). PMLs allow the outgoing acoustic waves to leave the modelling domain without reflections, thereby avoiding formation of standing waves.

The material properties of the piezoelectric material, housing material and encapsulation material used within the hydrophone are assigned based on material datasheets and relevant measurements. In this study, it is assumed that all materials including fluid and solid are homogeneous, isotropic and linear in nature whereas piezo electric material is assumed to be transversely isotropic. The FEM mesh was generated using tetrahedral elements with a size chosen to achieve a balance between accuracy and computational efficiency. While meshing for the acoustic analysis, it is to be ensured that the element size is small enough to resolve the waves or else the FEA would become inaccurate. Hence the structural and acoustic domains are meshed with 6 elements per wavelength($\lambda/6$). Swept mesh with 5 layers is used for the PML. Appropriate boundary conditions were applied to the model to simulate the experimental setups. For the structural analysis, the inner face of mounting holes on the ears of hydrophone is assigned as fixed support and the hydrophone is subjected to a harmonic base excitation load of 1g (refer Fig. 2). The frequency response of the hydrophone is studied across the operating band. For the acoustic analysis, the hydrophone is subjected to a harmonic plane wave of magnitude 1Pa with frequencies varying across the operating range and the response of the hydrophone is studied.

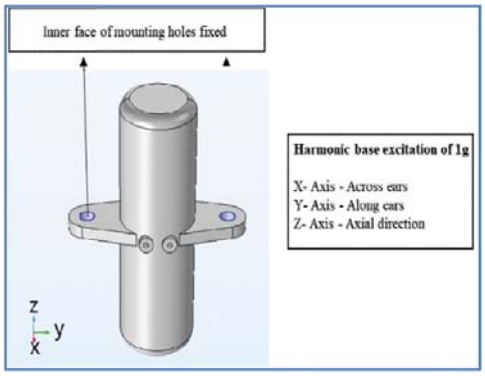

Fig. 2: Geometry model in COMSOL Multiphysics

Multiphysics capabilities of the FEM software were utilized for effectively capturing the complex interplay between piezoelectric elements and surrounding acoustic medium. These results are presented and compared with the measured data in the results section to assess the accuracy of the FEM model and its ability to predict the hydrophone's behavior.

5. RESULTS AND DISCUSSIONS

5.1 Comparison of FEM and measurement Results

A comparison study is conducted between measured data and corresponding FEM simulation results to assess the accuracy of FEM model in predicting hydrophone's acceleration and receiving sensitivities.

(a) ***Vibration measurements :*** The results from FEM model are compared with the measured data. It is observed that FEM model was able to capture the resonance frequencies of hydrophone along the three fundamental axes accurately. The FEM simulations predicted a similar trend in the acceleration sensitivity showing good qualitative correlation but varying degrees of quantitative agreement across the operating frequency range (as shown in Fig. 3). Specifically, while the acceleration sensitivity spectrum along X-axis shows strong magnitude agreement, Y &Z axes exhibit discrepancies. These quantitativediscrepancies are primarily due to assumptions made in frequency dependent properties of materials and the simplificationswithin the FEA model.

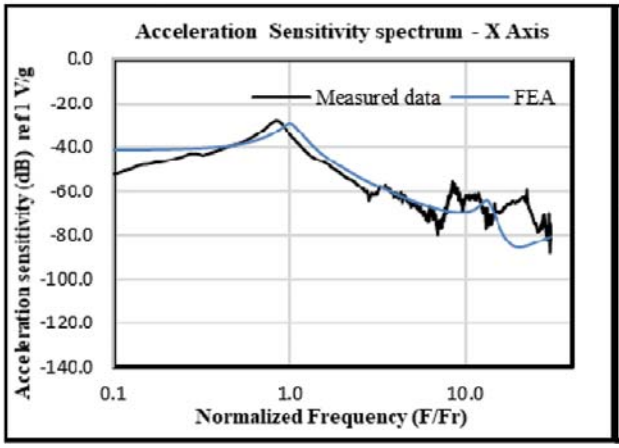

Fig. 3: (a) Acceleration sensitivity spectrum - X axis

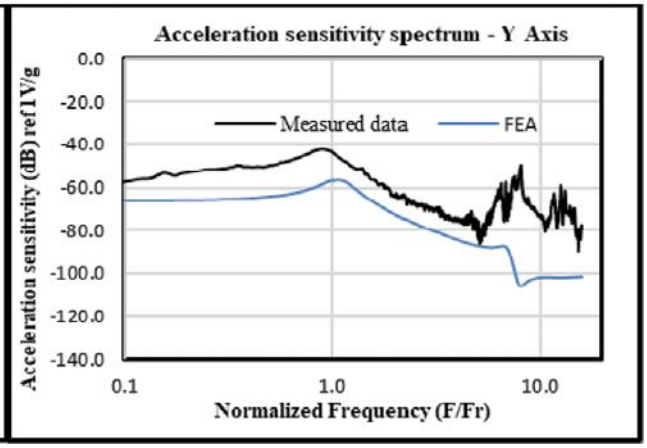

Fig. 3: (b) Acceleration sensitivity spectrum - Y axis

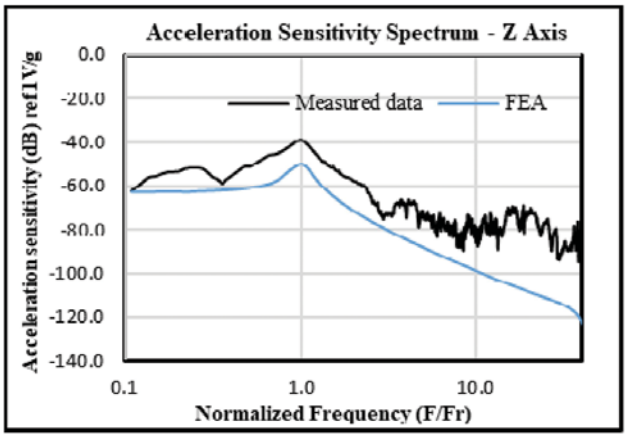

Fig. 3: (c) Acceleration sensitivity spectrum -Z axis

(b) ***Receiving sensitivity measurement :*** The measured receiving sensitivity of the hydrophone exhibited a flat response across frequency spectrum which is replicated by the FEM simulations (Fig. 4).

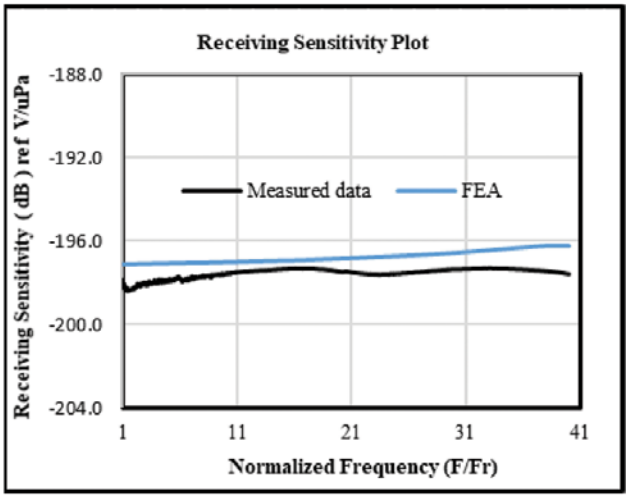

Fig. 4: Receiving sensitivity plot

Overall, the FEM model demonstrated a good capability in predicting the hydrophone's behaviour under both structural and acoustic excitation conditions. Good agreements between the experimental and simulation results validates the FEM model's fidelity and its potential for optimizing hydrophone design.

5.2 Different Mounting Setups

Fig. 5 depicts the variation in acceleration sensitivity across the operating frequency range for each setup. The results are juxtaposed with validated Finite element analysis (FEA) data for comparative analysis. No significant variation in acceleration sensitivity was observed in the radial direction (X and Y axis). However, a slight radial resonance frequency shifts were observed in the operating range. Additionally, a modest reduction in acceleration sensitivity is noted when the ears were excluded from the system.

Notably along axial direction (Z-axis), the configuration with the ear nut exhibits slightly higher acceleration sensitivity levels across the frequency range which is undesirable for the hydrophone. Eliminating the ears significantly reduced acceleration sensitivity levels across the frequency band, with

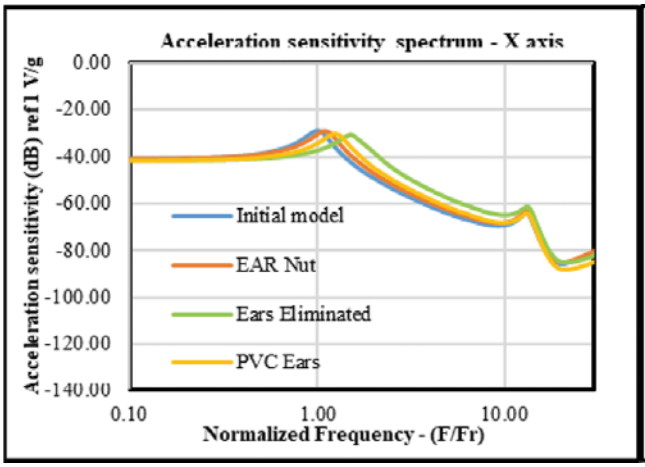

Fig. 5: (a) Acceleration sensitivity spectrum - X axis

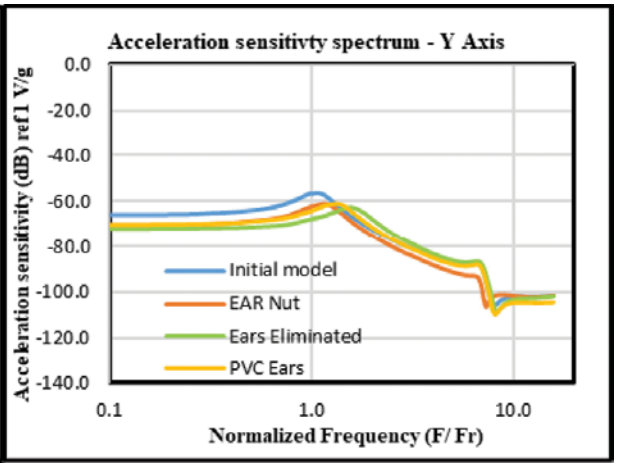

Fig. 5: (b) Acceleration sensitivity spectrum - Y axis

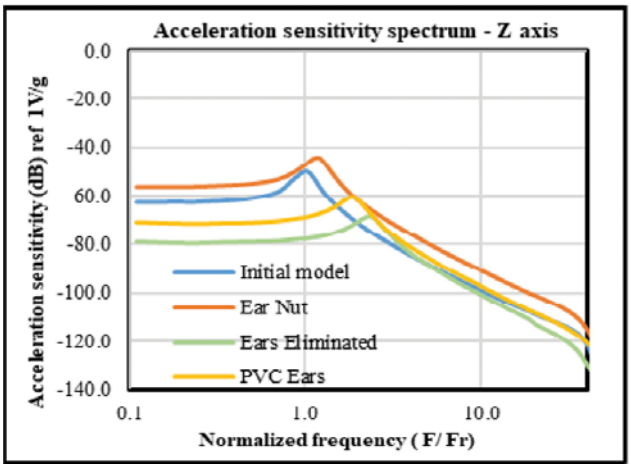

Fig. 5: (c) Acceleration sensitivity spectrum -Z axis

a flatter spectral profile. Even though the resonance frequencies are shifted to the working range, its effect is negated by the significant decrease in acceleration sensitivity. The PVC ears configuration also follows a similar trend in Z-axis as that of ears eliminated but the acceleration sensitivity level is higher on comparison with the ears eliminated configuration (Fig. 5).

No significant variation in receiving sensitivity is observed across the different mount configurations. This indicates that the hydrophone's mount design has negligible influence on its acoustic reception performance (Fig. 6).

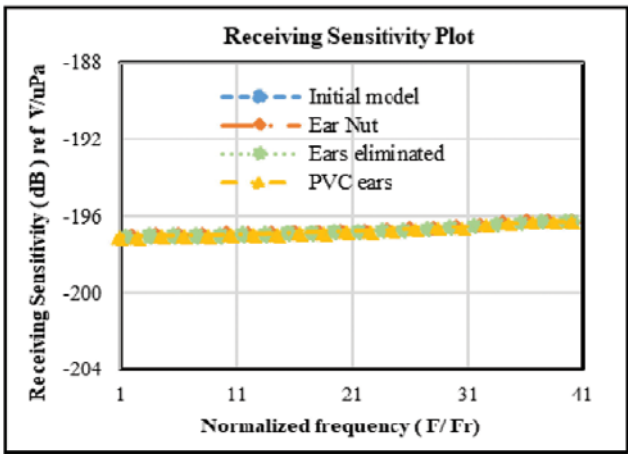

Fig. 6: Receiving sensitivity plot of different mount configuration

6. CONCLUSION

The finite element model developed using COMSOL Multiphysics demonstrated reasonable agreement with measured data, validating its accuracy in predicting the hydrophone's behavior under both vibro-electric and electro-acoustic studies.The vibro-electric analysis of different mounting configurations revealed a substantial impact on acceleration sensitivity along axial direction. The ear nut configuration exhibited higher acceleration sensitivity levels, potentially compromising the hydrophone's performance in high-vibration environments. While the elimination of ears led to the lowest acceleration levels. Although the resonance frequency experiences a less significant increase which can be overlooked by the reduction in relative magnitude of the acceleration sensitivity. Not much significant change is observed in radial direction.

Notably, the receiving sensitivity remained relatively consistent across different mounting configurations, suggesting that the receiving sensitivity of the hydrophone is not affected by mounting design compared to its vibrational response. These findings provide valuable insights into the design and optimization of hydrophone mounting systems for improved performance and durability. Future research could focus on developing innovative mounting solutions that balance acceleration sensitivity and other critical performance parameters.

REFERENCE

[1] Hamid Saheban and Zoheir Kordrostami, 2021. "Hydrophones, fundamental features, design considerations and various structures: A review. *Sensors and Actuators"*, A 329(2021) 112790.

[2] A. D. Waite, 2001. "Sonar for Practicing Engineers, 3rd edition", John Wiley & Sons Ltd., pp. 89-90.

[3] Matthew E. Schinault, Seth M. Penna and Heriberto A., 2019. "Investigation and Design of a Towable Hydrophone Array for General Ocean Sensing", OCEANS 2019–Marseille, Marseille, France, *IEEE*.

[4] Liang FENG, Shu-shu SI and Xin-ran XU., 2021. "Research on the influence of vibration environment on acoustic performance of hydrophone", 15th Symposium on Piezoelectricity, Acoustic waves and Device Applications, Zhengzhou China, *IEEE*, 2020.

[5] Guo YAN, Xin-ran XU, Zhen-yu ZHENG and Wei GAO, 2020, "Acceleration sensitivity analysis of hydrophone", 15th Symposium on Piezoelectricity, Acoustic waves and Device Applications, Zhengzhou China, *IEEE*, 2020.

[6] D. Stansfield, 1990. "Underwater Electroacoustic Transducers: A Handbook for users and designers", Bath university press, pp. 260, 307.

The Journal of Acoustical Society of India : Vol. 52, No. 4, 2025 (pp. 198-203)

AUV Mine Counter Measure approach using Content based Image Retrieval

Amit Kumar Verma

Research Centre Imarat, Hyderabad, India
e-mail: verma.amit.k@gmail.com

[Received: 01.09.2025; Revised: 11.11.2025; Accepted: 11.11.2025]

ABSTRACT

Navies around the world have successfully conducted underwater Mine Counter Measure (MCM) operations using Autonomous Underwater Vehicles (AUVs). Our proposed approach for detection, localization and classification of MLOs require better along track and across track resolution of the Side Imaging Sonar which can be obtained with Synthetic Aperture Sonar (SAS). The proposed MCM methodology consists of AUV Path Planning, which is done when the AUV is at the mother platform (ship). The current location of the AUV is updated (through GPS). Once the AUV dips into water, the inbuilt Inertial Navigation System (INS) updates the current location of the AUV. It is followed by Synthetic Aperture Sonar (SAS) scanning to obtain sonar image of the ocean floor. The sonar image so obtained is divided into small sub-images (of say 20m × 20m). The next stepsare Online Automatic Target Recognition (ATR) using Content Based Image Retrieval (CBIR), and Image Edge Detector; Content Based Image Retrieval (CBIR), which is based on feature extraction of each sub-image (query image) and conducting a similarity measure for matching an image from the database closest to the query image in terms of feature vector. If the image No. n belongs to the Mine Like Objects (MLOs) cluster in the database and is confirmed using sensors (like magnetometer), we consider this query image as a valid detection and do further processing. In Image Edge Detector, the sonar queryimage (validated as a mine) is then processed by Canny Edge Detector. This results in a low-resolution image (in kBs) compared to the high-resolution query image (in MBs).The last step consists of updating mother platform in real time with low resolution edge-detected image.The concept has been implemented in MATLAB and results are discussed.

1. INTRODUCTION

Underwater mines are designed to be undetectable and can float on top of a body of water, rest on the sea floor, or be moored to the sea floor.They can utilize acoustic sensors, pressure sensors, and a multitude of other techniques in order to become precise and lethal[1]. The detection of underwater mines from sonar returns is a challenging task which is further complicated by the variable and intricate backgrounds found on the seabed. Clearing a minefield can take up to 200 times longer and cost up to 200 times more than laying a minefield[2].

Autonomous Underwater Vehicles (AUVs) are being used successfully in underwater Mine Counter Measure (MCM) operations by Navies around the world. This approach reduces the risk to life of ship's crew by autonomously detecting and neutralizing mines while mother ship is at a safe standoff distance. For MCM operations, AUVs employ high frequency acoustic Side Imaging Sonars like Side Scan Sonar(SSS)

or Synthetic Aperture Sonar (SAS) to detect, classify, and localize Mine Like Objects (MLOs) on the ocean floor. The requirement of better along track and across track resolution can be met with SAS imagery as compared with SSS imagery. SAS can produce maps with centimetre level resolution and area coverage of better than one square km per hour[3].

The proposed MCM methodology consists of:

(a) AUV Path Planning,

(b) Synthetic Aperture Sonar(SAS) scanning,

(c) Online Automatic Target Recognition (ATR),

(d) Update mother platform in real time.

The paper is organised as follows. Section 2discusses AUV path planning. Sea bed scanning using Synthetic Aperture Sonar (SAS) is discussed in Section 3. In Section 4, Automatic Target Recognition (ATR) using 1) Content Based Image Retrieval (CBIR) and 2) Image Edge Detector is explained. Section 5 describes the process of updating the Mother platform (Ship) about presence of MLOs in real time.

2. AUV PATH PLANNING

The AUV path planning is done when the AUV is at the mother platform(ship). The current location of the AUV is updated (through GPS). Once the AUV dips into water, the inbuilt Inertial Navigation System (INS) updates the current location of the AUV. Depending upon the mission requirements, the AUV goes to a designated area and starts scanning the area.

Most research about path planning for AUVs deals with attempting to find a route that will allow an AUV to transit safely from one location to another, or through a series of waypoints. A detailed description and comparison of various path planning techniques is given in[4].

In the context of present paper, the objective of the path planning task is maximizing the success of detecting underwater mines. Path planning, in case ofMine Counter Measure (MCM) operations, is very different from the path planning done for the conventional AUVsbecause in the case of MCM operations, the route that the AUV takes will in turn, impact the data that is collected and subsequently analyzed. The path-planning approach widely used in practice for underwater mine detection operations is to design ladder survey with equidistant tracks over the mission area, as shown in Fig. 1. In the present work, ladder survey technique is employed because, for MCM operations,data collected by traversing parallel tracks is more preferable for processing through SAS imagery[5].

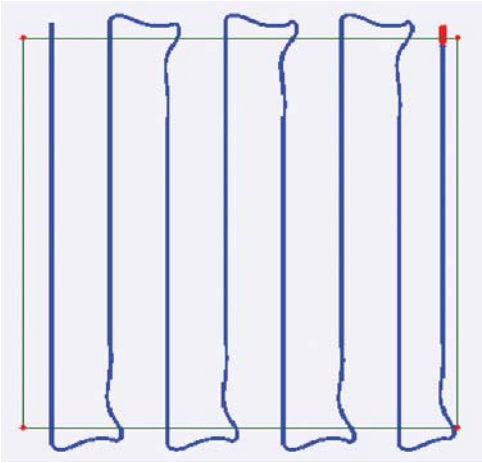

Fig. 1: Ladder survey technique for AUV path traversal.

AUV path planning along with AUV's restricted tolerance in pitch, roll and yaw (very accurate INS) is very critical for better SAS image formation.

3. SYNTHETIC APERTURE SONAR SCREENING

Synthetic Aperture Sonar (SAS) is used for high resolution underwater Imaging. Here a larger array is synthesised by using consecutive pings from the moving Sonar. It has a constant along track resolution, independent of frequency and distance. The AUV's scanning speed(v) depends on the Synthetic Aperture Sonar's swath coverage (R_{max}) andaperture length (d_a) and is expressed as

$$\left(\frac{2 * v}{d_a}\right) \leq \text{PRF} \leq \left(\frac{c}{2 * R_{\max}}\right) \tag{1}$$

Fig. 2. depicts the above relation.

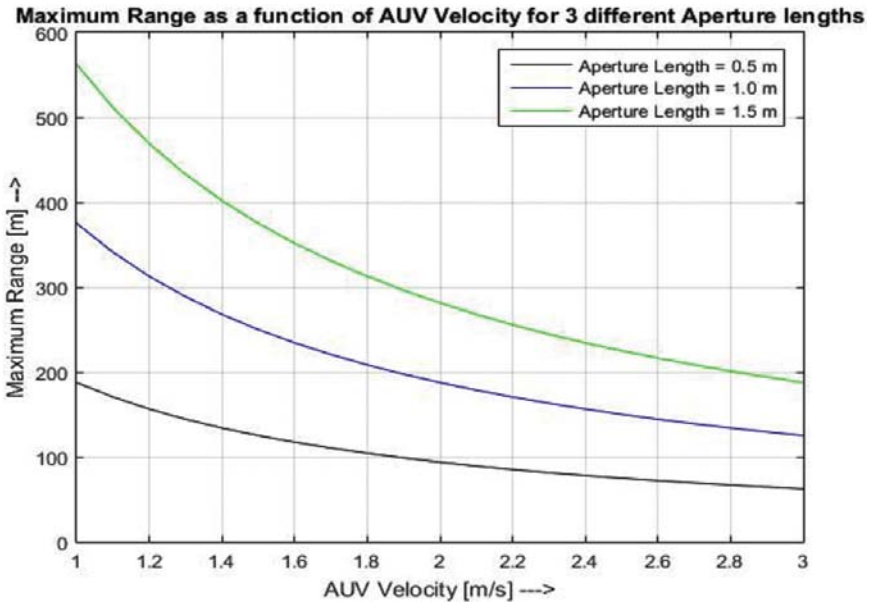

Fig. 2: Relation between AUV speed, swath coverage and aperture length of SAS.

SAS scanning produces images of the sea bed along with Mine Like Objects(MLOs). Such images are then subdivided into small sub-images as shown in Fig. 3.

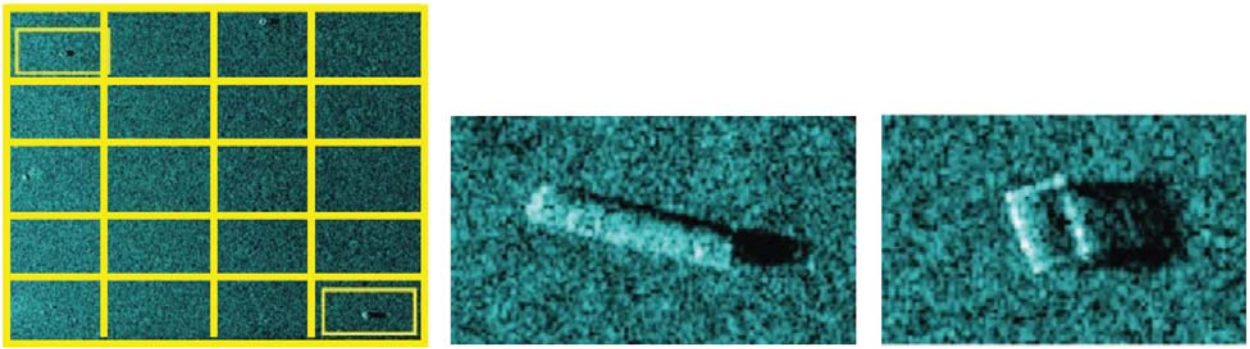

Fig. 3: SAS Image subdivided into sub-image 1 and sub-image *n*.

4. AUTOMATIC TARGET RECOGNITION

Online Automatic Target Recognition(ATR) is done using 1) Content Based Image Retrieval(CBIR), and 2) Image Edge Detector on the SAS sub-images.

4.1 Content Based Image Retrieval (CBIR)

CBIR is based on (i) feature extraction of each sub-image (query image) and (ii) conducting a similarity measure for matching an image from the database closest to the query image in terms of feature vector as depicted in Fig. 4.

Given, F = image space, X = feature space

$$f: F \rightarrow X,\ X = \{x_1, x_2, \ldots\ldots\ldots\ldots, x_n\} \tag{2}$$

Given a query image P, retrieve an image M from image database S such that

$$D(f(P), f(M)) \leq D(f(P), f(F), F \in S \tag{3}$$

An essential requirement of CBIR is the availability of a very extensive feature rich database of SAS images. This is required in the training/learning phase(done offline before AUV mission) of CBIR. We have taken SAS sonar images of Mine Like Objects (MLOs) available freely online. Due to limited availability of such sonar images and to make an extensive feature-rich database, we have also used some optical images of similar objects in the database. We have considered a weighted combination of features like texture, shape, mathematical moments, spatial relationships, etc. to make the feature vector.

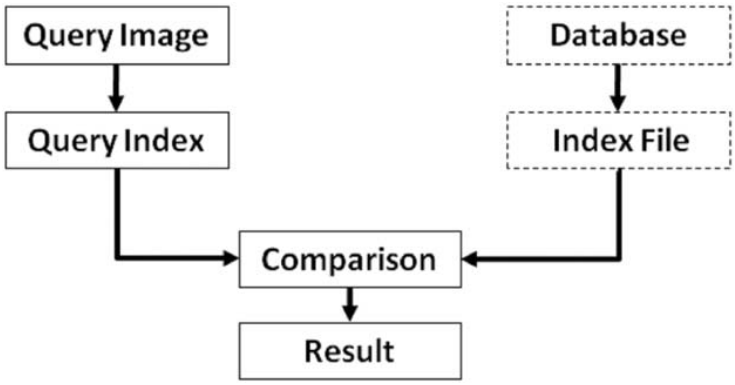

Fig. 4: CBIR Overview.

The output of CBIR processing is the sonar image(say image no. n) from the database closest to the query image in terms of the feature vector. We have the prior information about the image no. n (which was processed offline during the training phase). If the image no. n belongs to the Mine Like Objects (MLOs) cluster in the database, we consider this query image as a valid detection and do further processing. This has been implemented in Matlab[6] and training of the algorithm with the database has been done offline.

The above information is then confirmed with a magnetometer sensor output of the AUV. If both the data indicate positive presence of mine, a decision about presence of mine is taken online by the AUV.

4.2 Image Edge Detector

The sonar query image (validated as a mine) is then processed by Canny Edge Detector.This results in a low-resolution image (in kBs) compared to the high-resolution query image (in MBs) as shown in Fig. 5.

Canny Edge Detector method uses two thresholds to detect strong and weak edges and includes the weak edges in the output only if they are connected to strong edges[7]. The Matlab results are shown in Fig. 5.

5. UPDATE MOTHER PLATFORM IN REAL TIME

The low-resolution edge-detected image (in kBs) is then transmitted through underwater acoustic communication(low bandwidth channel) to the mother platform along with location of the mine (from INS data).

In case of unavailability of the above channel, the AUV periodically surfaces and transmits high resolution sub-image (in MBs) to mother platform using high bandwidth Line of Sight (LoS) communication as illustrated in Fig. 5. If this channel is also not available, the Satellite Communication (low bandwidth channel) is used to transmit the low-resolution edge-detected image (in kBs) and location of the suspected mine to the mother platform for further action.

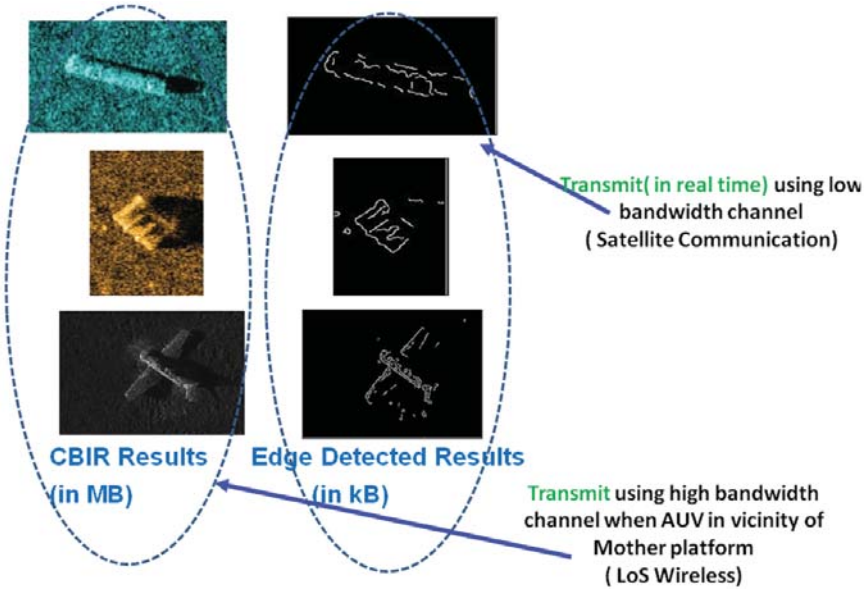

Fig. 5: Image Edge Detection (Canny) Results.

6. CONCLUSIONS

This paper describes an approach for Mine Counter Measures in AUV applications. The proposed approach consists of AUV's Path planning, Synthetic Aperture Sonar (SAS) scanning, Automatic Target Recognition and updating the mother platform in real time. The Post Processing is done using CBIR and Canny Edge Detector and has been implemented in Matlab. The performance of the Post Processing algorithms depends to a large extent on the quality of features-rich database. Due to non-availability of extensive SAS images of targeted objects, optical images of the targeted objects were also used in the database along with SAS images to convey the approach. Further studies on the image featuresrelevant to SAS imagery is expected to optimise the performance of the Post Processing approach.

REFERENCES

[1] T. Brown *et al.*, 2012. *Next Generation Mine Countermeasures for the Very Shallow Water Zone in Support of Amphibious*, Naval Postgraduate School, Monterrey, CA.

[2] Siamak Khaledi, Hari Mann, James Perkovich and Samar Zayed, 2014. Design of an underwater mine detection system,*IEEE Symposium on Systems and Information Engineering Design*, 2014, Charlottesville, VA, USA, 25 April, (2014).

[3] Roy Edgar Hansen, *et al.*, 2008. High Fidelity Synthetic Aperture Sonar (S.A.S) products for target Analysis, *IEEE Oceans 2008*, Quebec. Canada.

[4] Konuralp Yigit, 2011. *Path Planning Methods for Autonomous Underwater Vehicles*, Master of Science Thesis in Naval Architecture and Marine Engineering,Massachusetts Institute of Technology.

[5] David P. Williams, 2010. On Optimal AUV Track-Spacing for Underwater Mine Detection,*IEEE International Conference on Robotics and Automation*, 2010, Anchorage, AK, USA, 03–07 May, (2010).

[6] The Mathworks, Inc. (2022). *MATLAB version: 9.13.0 (R2022b).* Accessed: January 01, 2023.Available: https://www.mathworks.com

[7] John Canny, 1986. A Computational Approach to Edge Detection, *IEEE Transactions on Pattern Analysis and Machine Intelligence*, **8**(6): 679–697.

INFORMATION FOR AUTHORS

ARTICLES

The Journal of Acoustical Society of India (JASI) is a refereed publication published quarterly by the Acoustical Society of India (ASI). JASI includes refereed articles, technical notes, letters-to-the-editor, book review and announcements of general interest to readers.

Articles may be theoretical or experimental in nature. But those which combine theoretical and experimental approaches to solve acoustics problems are particularly welcome. Technical notes, letters-to-the-editor and announcements may also be submitted. Articles must not have been published previously in other engineering or scientific journals. Articles in the following are particularly encouraged: applied acoustics, acoustical materials, active noise & vibration control, bioacoustics, communication acoustics including speech, computational acoustics, electro-acoustics and audio engineering, environmental acoustics, musical acoustics, non-linear acoustics, noise, physical acoustics, physiological and psychological acoustics, quieter technologies, room and building acoustics, structural acoustics and vibration, ultrasonics, underwater acoustics.

Authors whose articles are accepted for publication must transfer copyright of their articles to the ASI. This transfer involves publication only and does not in any way alter the author's traditional right regarding his/her articles.

PREPARATION OF MANUSCRIPTS

All manuscripts are refereed by at least two referees and are reviewed by the Publication Committee (all editors) before acceptance. Manuscripts of articles and technical notes should be submitted for review electronically to the Chief Editor by e-mail or by express mail on a disc. JASI maintains a high standard in the reviewing process and only accept papers of high quality. On acceptance, revised articles of all authors should be submitted to the Chief Editor by e-mail or by express mail.

Text of the manuscript should be double-spaced on A4 size paper, subdivided by main headings-typed in upper and lower case flush centre, with one line of space above and below and sub-headings within a section-typed in upper and lower case understood, flush left, followed by a period. Sub-sub headings should be italic. Articles should be written so that readers in different fields of acoustics can understand them easily. Manuscripts are only published if not normally exceeding twenty double-spaced text pages. If figures and illustrations are included then normally they should be restricted to no more than twelve-fifteen.

The first page of manuscripts should include on separate lines, the title of article, the names, of authors, affiliations and mailing addresses of authors in upper and lowers case. Do not include the author's title, position or degrees. Give an adequate post office address including pin or other postal code and the name of the city. An abstract of not more than 200 words should be included with each article. References should be numbered consecutively throughout the article with the number appearing as a superscript at the end of the sentence unless such placement causes ambiguity. The references should be grouped together, double spaced at the end of the article on a separate page. Footnotes are discouraged. Abbreviations and special terms must be defined if used.

EQUATIONS

Mathematical expressions should be typewritten as completely as possible. Equation should be numbered consecutively throughout the body of the article at the right hand margin in parentheses. Use letters and numbers for any equations in an appendix: Appendix A: (A1, (A2), etc. Equation numbers in the running text should be enclosed in parentheses, i.e., Eq. (1), Eqs. (1a) and (2a). Figures should be referred to as Fig. 1, Fig. 2, etc. Reference to table is in full: Table 1, Table 2, etc. Metric units should be used: the preferred from of metric unit is the System International (SI).

REFERENCES

The order and style of information differs slightly between periodical and book references and between published and unpublished references, depending on the available publication entries. A few examples are shown below.

Periodicals:

[1] S.R. Pride and M.W. Haartsen, 1996. Electroseismic wave properties, *J. Acoust. Soc. Am.*, **100** (3), 1301-1315.

[2] S.-H. Kim and I. Lee, 1996. Aeroelastic analysis of a flexible airfoil with free play non-linearity, *J. Sound Vib.*, **193** (4), 823-846.

Books:

[1] E.S. Skudzryk, 1968. *Simple and Comlex Vibratory Systems*, the Pennsylvania State University Press, London.

[2] E.H. Dowell, 1975. *Aeroelasticity of plates and shells*, Nordhoff, Leyden.

Others:

[1] J.N. Yang and A. Akbarpour, 1987. Technical Report NCEER-87-0007, Instantaneous Optimal Control Law For Tall Buildings Under Seismic Excitations.

SUMISSIONS

All materials from authors should be submitted in electronic form to the JASI Chief Editor: B. Chakraborty, CSIR - National Institute of Oceanography, Dona Paula, Goa-403 004, Tel: +91.832.2450.318, Fax: +91.832.2450.602,(e-mail: bishwajit@nio.org) For the item to be published in a given issue of a journal, the manuscript must reach the Chief Editor at least twelve week before the publication date.

SUMISSION OF ACCEPTED MANUSCRIPT

On acceptance, revised articles should be submitted in electronic form to the JASI Chief Editor (bishwajit@nio.org)